ARMY RESEARCH LABORATORY

AN ATMOSPHERIC BOUNDARY LAYER STABILITY ESTIMATOR FOR URBAN AREAS

SBIR PHASE I FEASIBILITY STUDY

J. S. Scire
S. R. Hanna

Sigma Research Corporation
196 Baker Avenue
Concord, MA 01742

Under Contract DAAD07-91-C-0135
Contract Monitor Frank V. Hansen

ARL-CR-10 *December 1992*

Approved for public release; distribution unlimited.

NOTICES

Disclaimers

The findings in this report are not to be construed as an official Department of the Army position, unless so designated by other authorized documents.

The citation of trade names and names of manufacturers in this report is not to be construed as official Government indorsement or approval of commercial products or services referenced herein.

Destruction Notice

When this document is no longer needed, destroy it by any method that will prevent disclosure of its contents or reconstruction of the document.

REPORT DOCUMENTATION PAGE

Form Approved
OMB No. 0704-0188

1. AGENCY USE ONLY (Leave blank)	2. REPORT DATE	3. REPORT TYPE AND DATES COVERED
	December 1992	Final

4. TITLE AND SUBTITLE

AN ATMOSPHERIC BOUNDARY LAYER STABILITY ESTIMATOR FOR URBAN AREAS - SBIR PHASE I FEASIBILITY STUDY

5. FUNDING NUMBERS

61102/B53A (6.1)

6. AUTHOR(S)

J. S. Scire and S. R. Hanna

7. PERFORMING ORGANIZATION NAME(S) AND ADDRESS(ES)

Sigma Research Corporation
196 Baker Avenue
Concord, MA 01742

8. PERFORMING ORGANIZATION REPORT NUMBER

ARL-CR-10

9. SPONSORING/MONITORING AGENCY NAME(S) AND ADDRESS(ES)

U.S. Army Research Laboratory
Battlefield Environment Directorate
White Sands Missile Range, NM 88003-5501

10. SPONSORING/MONITORING AGENCY REPORT NUMBER

11. SUPPLEMENTARY NOTES

Frank V. Hansen (Contract Monitor)

12a. DISTRIBUTION/AVAILABILITY STATEMENT

Approved for public release; distribution unlimited.

12b. DISTRIBUTION CODE

13. ABSTRACT (Maximum 200 words)

In most U.S. Army atmospheric dispersion models, the Pasquill methodology is used to estimate stability in the boundary layer. As a result, there are discontinuities in calculated dispersion among the six stability classes. Furthermore, corrections for surface conditions (i.e., fields, urban areas, or forests) are also discrete functions. Recent theoretical developments provide the basis for revising this methodology using principles of Monin-Obukhov and convective similarity theory. A model is described which predicts stability indicators in a continuous manner. The procedure consists of three components: a soil moisture module to predict surface moisture; a meteorological module, based on an energy balance method, to predict surface energy fluxes and boundary layer parameters; and a set of similarity relations to estimate atmospheric stability and plume dispersion parameters. The model is designed for PC use and requires only routinely available meteorological and land use data.

14. SUBJECT TERMS

Atmospheric stability, urban boundary layer, stability estimator, turbulence

15. NUMBER OF PAGES

82

16. PRICE CODE

17. SECURITY CLASSIFICATION OF REPORT	18. SECURITY CLASSIFICATION OF THIS PAGE	19. SECURITY CLASSIFICATION OF ABSTRACT	20. LIMITATION OF ABSTRACT
Unclassified	Unclassified	Unclassified	SAR

TABLE OF CONTENTS

1. INTRODUCTION

Most diffusion models applied by the Department of Defense, the Environmental Protection Agency (EPA), and other government agencies are based on the 30-year-old Pasquill stability category methodology, whose six stability classes are determined as a function of wind speed, solar elevation angle, and cloudiness. Slightly different methods are used for rural and urban areas, but there is no continuous variation between the two surface or between stability classes for the same surface. As a result, predicted pollutant concentrations are discontinuous functions of the six stability classes and two types of surfaces.

In 1977, the American Meteorological Society convened a workshop on stability classification schemes which recommended that advances in boundary layer theory be used to revise the discrete stability class methodology (Hanna et al., 1977). Recent advances in convective scaling have since developed to provide a better basis for analyzing dispersion in the convective boundary layer. This Phase I research is intended to outline the structure of a new methodology for predicting continuous stability indicators based on the current state-of-the-science. The algorithms, intended for implementation on a personal computer, require only routinely available meteorological observations and land use categorizations. The formulation of the model is general. It is equally valid over rural areas or urban environments as long as the proper model inputs are specified.

The model consists of three components. The first component is a soil moisture module which uses precipitation observations and land use characteristics to predict the important surface moisture parameter. A new capacitance method for determining surface moisture has been developed for this project. Its characteristics have been compared against two more complex numerical soil moisture models and it has been used to simulate moisture in both rural and urban environments for a three month period in order to illustrate the technique in an operational mode. The topic of moisture availability is discussed in Section 2.3

The second component of the model is a meteorological preprocessor which uses observations of wind speed and direction at a height of 10 m, cloud cover, surface characteristics, and surface moisture predicted by the capacitance model to determine the surface sensible and latent heat fluxes, surface friction velocity, Monin-Obukhov length, and convective velocity scale. These variables are important boundary layer parameters which determine atmospheric turbulence and dispersion rates. If mixing heights are to be predicted, the model also requires temperature sounding data. The meteorological preprocessor is based on an energy balance method, described in Sections 2.1 and 2.2. The parameterizations of the boundary layer parameters are described in Section 2.4.

The third component of the model is a series of similarity relations which determine plume dispersion parameters, σ_y and σ_z, as a function of the boundary layer parameters. Unlike tradition dispersion curves, the dispersion parameters vary in a continuous manner as a function of plume height, atmospheric stability, and surface characteristics. The similarity relationships are equally applicable over urban, suburban and rural areas. The dispersion component of the model is described in Section 3.

Finally, a summary of the conclusions and recommendations for future Phase II research are described in Section 4.

2. SURFACE ENERGY BUDGET AND BOUNDARY LAYER PARAMETERS

A number of significant advances have been made in recent years in the understanding and characterization of the structure of the planetary boundary layer (PBL) (e.g., Hanna et al., 1977; Weil, 1985; Briggs, 1985). The use of appropriate boundary layer scaling parameters, which provides a continuous representation of stability and dispersion in the atmosphere, can improve the quality of dispersion predictions (e.g., van Ulden and Holtslag, 1985). The principal parameters needed to describe the boundary layer structure are the surface heat flux, surface momentum flux, and the boundary layer height. Several additional parameters, including the friction velocity, convective velocity scale, and the Monin-Obukhov length are derived from the primary parameters.

As part of the Electric Power Research Institute (EPRI) Advanced Plume project, Hanna et al. (1986) evaluated several models for the prediction of these boundary layer parameters from routinely-available meteorological observations. Two basic methods are commonly used to estimate boundary layer parameters such as surface heat and momentum fluxes. The first method is referred to as the profile method. It requires at a minimum observations of the wind speed at one height and the temperature difference between two heights in the surface layer, as well as knowledge of the air temperature and roughness characteristics of the surface. Monin-Obukhov similarity theory is then used to solve the surface energy fluxes by iteration. The second approach, called the energy budget method, computes the surface heat flux by parameterizing the various terms of the surface energy budget equation.

Hanna et al. (1986) tested and intercompared four energy budget models (Holtslag and van Ulden, 1983; Weil and Brower, 1983; Berkowicz and Prahm, 1982; and Briggs, 1982) and two profile schemes (two-level tower method and four-level tower method). A major conclusion of the study was that the energy budget methods were superior over land surfaces because of the high sensitivity of the profile method to small errors in the measured temperature difference. In addition, the four different energy budget methods performed with similar skill. For this reason, the energy budget method was selected as the basis for estimating the required urban energy balance and boundary layer parameters.

2.1 Urban Surface Energy Budget

The energy balance at the surface can be written as:

$$Q_* + Q_f = Q_h + Q_e + Q_g + Q_a \qquad (1)$$

where Q_* is the net all-wave radiation,
Q_f is the anthropogenic heat flux,
Q_h is the sensible heat flux,
Q_e is the latent heat flux,
Q_g is the ground/storage heat flux, and,
Q_a is the net heat advection.

Urbanization changes the properties of the surface and atmosphere in several important ways which must be included in the parameterization of the various terms of the energy balance equation. For example, the aerodynamic, thermal, hydrological, and radiative characteristics of the surface are changed as a result of urbanization (Oke, 1978). These changes have important effects on atmospheric stability and turbulence in the urban environment. For example, buildings and other obstacles to the wind flow create a very rough surface which increases the mechanically generated atmospheric turbulence in the lowest layer of the atmosphere. Briggs (1983) estimates increases in the surface friction velocity of 30-50% in urban areas relative to surrounding suburban and rural areas. The thermal properties of the urban surface are altered by the presence of dense building materials which efficiently store heat. In addition, anthropogenic heat sources can contribute significantly to the urban energy budget. The large fraction of the urban surface impervious to water and urban runoff routing systems affect the available moisture and therefore, the partitioning of available energy into sensible and latent heat fluxes. Godowitch et al. (1981), White et al. (1978), Hildebrand and Ackerman (1984) and others report urban sensible heat fluxes 2-4 times higher than those in nearby rural areas. In addition, urban areas tend to have higher concentrations of atmospheric pollutants, which alters the spectrum and intensity of solar radiation received at the surface (Landsberg, 1981).

Cleugh and Oke (1986) present simultaneous energy balance observations at rural and suburban sites in Vancouver, B.C. which illustrate some of the effects of urbanization. The major components of the energy balance equation are shown in Figure 1 averaged over a period of 30 days during the summer of 1983 for both sites. In the suburban area, the net radiation increased 4%, the sensible heat flux increased 51%, and the latent heat flux decreased 46% as compared to the rural values. The Bowen ratio (ratio of sensible to latent heat flux) averaged 0.5 in the rural area and 1.3 in the suburban area, reflecting decreased moisture availability in the suburban environment.

The energy budget methodology provides a general framework for predicting energy fluxes, and profiles of winds, temperature, and turbulence which is valid for all types of underlying surfaces. By properly defining the surface characteristics and related parameters, the energy budget technique can be used to derive estimates of atmospheric stability and plume dispersion parameters which are continuous in both space and time for surfaces ranging from highly urbanized to suburban to rural land use.

2.2 Parameterization of the Terms of the Surface Energy Budget Equation

The solution of the energy budget equation is based primarily on the methods of Holtslag and van Ulden (Holtslag and van Ulden, 1983; van Ulden and Holtslag, 1985). The energy budget equation is solved for the sensible heat flux by parameterizing the other terms of the equation in terms of known quantities. Meteorological preprocessors implementing these techniques for urban areas have been developed and applied by Scire et al. (1986) (used predicting plume dispersion and dry deposition rates in New York City) and Hanna and Chang (1991 and 1992) (as part of the HPDM-Urban model development and evaluation program).

The parameterization of the various energy budget terms is described below.

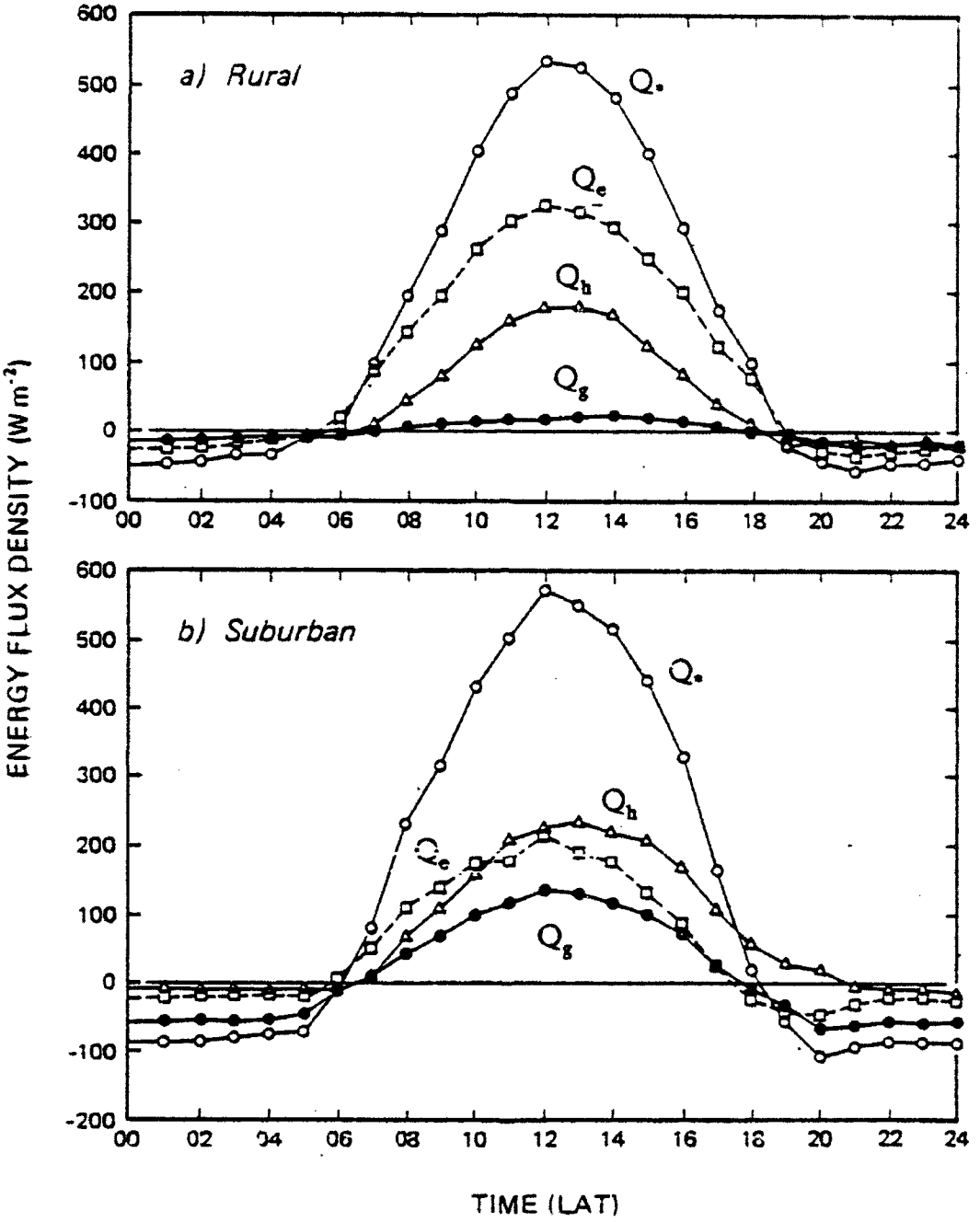

Figure 1. Variation of average energy balance components for (a) rural and (b) suburban sites in Vancouver, B.C. for 30 summer days in 1983. Q_* is net radiation flux, Q_h is sensible heat flux, Q_e is latent heat flux, and Q_g is ground heat flux. (From Cleugh and Oke, 1986.)

NET RADIATION

The net radiation, Q_*, is computed as the residual of incoming (short-wave plus long-wave) radiation and outgoing (long-wave) radiation. It can be expressed (Holtslag and van Ulden, 1983; Landsberg, 1981) as:

$$Q_* = (1-A)Q_{sw} + Q_{lw-d} - Q_{lw-u} \qquad (2)$$

where Q_{sw} is the incoming short-wave radiation (W/m^2), consisting of a direct solar radiation term (Q_{sw-s}) plus a diffuse radiation term (Q_{sw-d}),
A is the albedo of the surface,
Q_{lw-d} is the incoming long-wave atmospheric radiation (W/m^2), and,
Q_{lw-u} is the long-wave radiation (W/m^2) emitted by the surface.

Both components of the short-wave radiation term are altered by conditions in the urban environment. Direct solar radiation, Q_{sw-s}, is substantially decreased due to attenuation by urban air pollutants. Typically, Q_{sw-s} is about 40% less in urban areas than in surrounding rural areas (Unsworth and Monteith, 1972). The ultraviolet (UV) portion of the spectrum is affected much more than the longer wavelengths. However, diffuse radiation, Q_{sw-d}, is increased in urban areas. The net effect is that Q_{sw} is typically 10-20% less in urban areas (Oke, 1978; Landsberg, 1981). Another mitigating factor in the net radiation budget is that urban areas generally have lower surface albedos than most rural environments, and thus lower losses of short-wave radiation due to reflection from the surface. For example, typical urban albedos in St. Louis are 0.12-0.13 whereas albedos in the surrounding rural land surfaces are 0.15-0.17 (White et al., 1978).

The individual long-wave terms of the net radiation equation are also affected in an urban area. The warmer urban surface temperatures increase the emitted long-wave radiation (Q_{lw-u}). However, the incoming long-wave atmospheric radiation (Q_{lw-d}) is also increased due to higher pollutant levels. The net effect during the day is usually a slightly smaller long-wave loss in the urban area. At night, the long-wave loss is slightly larger in the urban area compared to rural areas (Oke, 1978).

Although each component of the net radiation (Q_*) equation is altered by urban conditions, the overall net effect is that the urban Q_* is usually not substantially different (i.e., is within about 5%) in mid-latitude cities from that in the surrounding rural areas (Oke, 1978; White et al., 1978). However, Oke (1978) points out exceptions such as in snow covered conditions or in cities in desert areas, where the rural albedo may be significantly higher. For example, typical albedos are in the range 0.40 to 0.95 over rural snow covered surfaces (Oke, 1978) and 0.20 to 0.45 in desert areas (Hanna and Chang, 1991). Snow in urban areas is usually quickly removed by plowing or salting operations, and tends not to stick to the vertical faces of buildings. Also, the snow melts faster due to the urban heat island effect. The urban snow that does remain tends to have a lower albedo due to soiling by urban pollution. In situations such as these, where the urban albedo is much lower than that in the surrounding rural areas, the term $(1-A)Q_{sw}$ can be substantially higher in the urban area, leading to higher urban values of net radiation.

Holtslag and van Ulden (1983) provide the following parameterizations of the short-wave and long-wave radiation terms in the net radiation equation:

$$Q_* = \frac{(1-A)Q_{sw} + c_1T^6 + c_2N - \sigma T^4}{1 + c_3} \qquad (3)$$

$$Q_{sw} = (a_1 \sin\phi + a_2)(1 + b_1 N^{b2}) \qquad (4)$$

$$c_3 = 0.38 \left[\frac{(1-\alpha)(S) + 1}{S + 1} \right] \qquad (5)$$

where T is the measured air temperature (deg. K),

σ is the Stefan-Boltzmann constant (5.67×10^{-8} W/m^2/deg. K^4),

N is the fraction of the sky covered by clouds,

ϕ is the solar elevation angle (deg.),

α is an empirical surface moisture parameter, and,

S is the slope of the saturation enthalpy curve [$S=s/\gamma$], where $s=\partial(q_s)/\partial(T)$ and $\gamma=c_p/L$,

λ is the latent heat of water vaporization.

q_s is the saturation specific humidity, and,

c_p is the specific heat at constant pressure.

The four terms in the numerator of Eqn. (3) account for absorption of short-wave radiation at the surface, incoming long-wave radiation from gaseous components of the atmosphere (e.g., water vapor and carbon dioxide), incoming long-wave radiation due to clouds, and outgoing long-wave radiation from the surface, respectively. The factor in the denominator $(1+c_3)$, results fr a the use of air temperature rather than the more difficult-to-determine surface radiation temperature in the equation. The term in the first set of parentheses in Eqn. (4) represents short-wave solar radiation in the absence of clouds. The second term $(1+b_1N^{b2})$, accounts for the reduction of incoming solar radiation due to clouds (b_1 is negative). The values for the empirical constants c_1, c_2, a_1, a_2, b_1, and b_2 suggested by Holtslag and van Ulden (1983) are shown in Table 1. It must be stressed that these "constants" were derived from observations in the Netherlands and may be expected to vary somewhat at other geographic locations characterized by different land use patterns, cloud types, and solar elevation angles. Furthermore, note that, in this system, clouds are parameterized by a single number, N, which is the fractional cloud cover. The system does not account for type, elevation, and density of clouds. Perhaps in the future, field data can be used to refine these parameterizations.

The parameter, S, describes the slope of the curve in the so-called Clausius-Clapeyron diagram, which is a fixture in introductory dynamic meteorology textbooks. Table 2 contains values of S as a function of T (in 5°C increments), for a pressure of 1000 mb.

The term $(1+c_3)^{-1}$ of Eqn. (3), which scales the net radiation, depends on both the ambient temperature and the surface moisture parameter. As shown in Figure 2, its sensitivity to soil moisture increases at higher temperatures. At 35°C, $(1+c_3)^{-1}$ increases about 47% from very dry to very wet conditions (i.e. α ranging from 0.0 to 1.4), but increases only about 36% for the same range of α at 20°C, and 19% at 0°C. Over a typical range of conditions expected at a single site, the sensitivity of net radiation to variations in $(1+c_3)^{-1}$ is more of the order of 20-30%.

Table 1

Values of Net Radiation Constants
(Holtslag and van Ulden, 1983)

Constant	Value
a_1	990 W/m^2
a_2	-30 W/m^2
b_1	-0.75
b_2	3.4
c_1	5.31×10^{-13} $W/m^2/deg.\ K^6$
c_2	60 W/m^2

Table 2

Slope of the Saturation Enthalpy Curve,

$S = (\partial q_s/\partial T)(L/c_p)$

as a Function of Temperature for a

Standard Pressure of 1000 mb.

(Holtslag and van Ulden, 1983)

T (°C)	S
-5	0.498
0	0.694
5	0.943
10	1.27
15	1.67
20	2.22
25	2.86
30	3.70
35	4.76

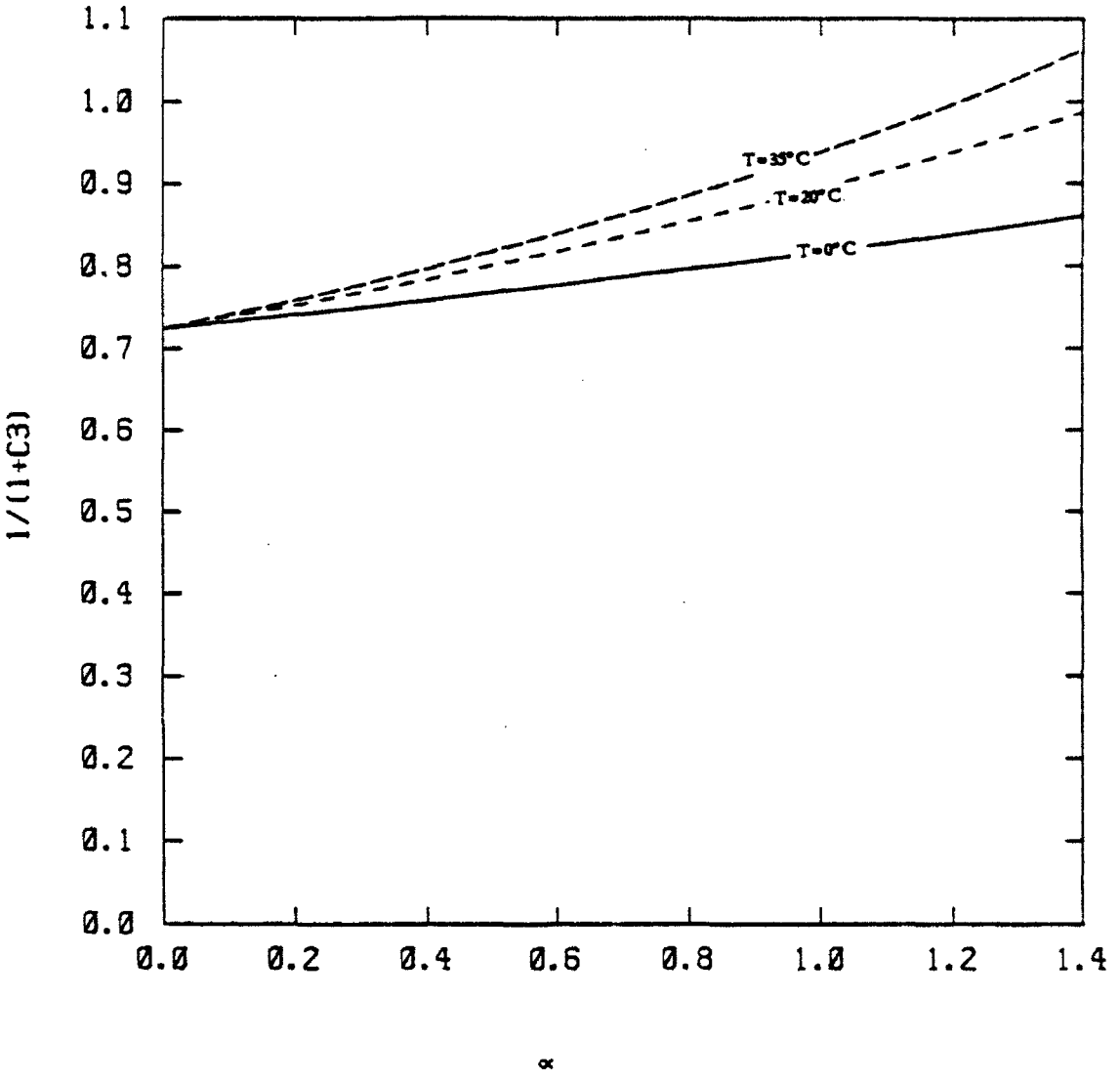

Figure 2. Plot of the term $(1+c_3)^{-1}$ of the net radiation equation as a function of the surface moisture parameter for three values of temperature.

The short-wave radiation, Q_{sw}, as predicted by Eqn. (4) is plotted as a function of time of day in Figure 3. The short-wave radiation data is computed for a latitude of 40° N for total cloud covers of 0, 0.50, 0.75, and 1.0 on two days of the year (winter solstice and summer solstice). Less than a 4% reduction in solar radiation is indicated for a cloudiness factor, N, up to 0.50. During overcast conditions (N = 1.0), the short-wave radiation is reduced to 0.25 of the clear-sky value.

Although the surface albedo, A, is nearly constant for high solar elevation angles (i.e., greater than 30°), it increases for lower angles (Coulson and Reynolds, 1971; Iqbal, 1983). Hanna and Chang (1991) recommend the use of the following relationship based on Iqbal (1983) for estimating the surface albedo as a function of elevation angle.

$$A = A' + (1-A')\, e^{a\phi+b} \tag{6}$$

$$b = -0.5\,(1-A')^2 \tag{7}$$

where A' is the albedo for the sun directly overhead,
ϕ is the solar elevation angle (degrees), and,
a is an empirical constant (~ 0.1).

ANTHROPOGENIC HEAT FLUX

In urban areas with high population densities and/or high per capita energy usage, the heat generated by man-made sources can significantly affect the overall energy budget. Table 3 shows the average anthropogenic heat flux (Q_f) and net radiation (Q_*) from several urban areas. Anthropogenic heat from sources such as space heating/cooling, transportation, and industrial facilities sometimes exceeds, on an annual basis, the energy input from net radiation (e.g., in Manhattan and Montreal). In densely populated northern cities, seasonal values of Q_f sometimes exceed Q_* by a large margin. For example, in Montreal, the average wintertime Q_f is 153 W/m^2, compared to a value of Q_* of 13 W/m^2.

The patterns of anthropogenic heat generation vary considerably depending on climatological factors. The ratio of wintertime anthropogenic

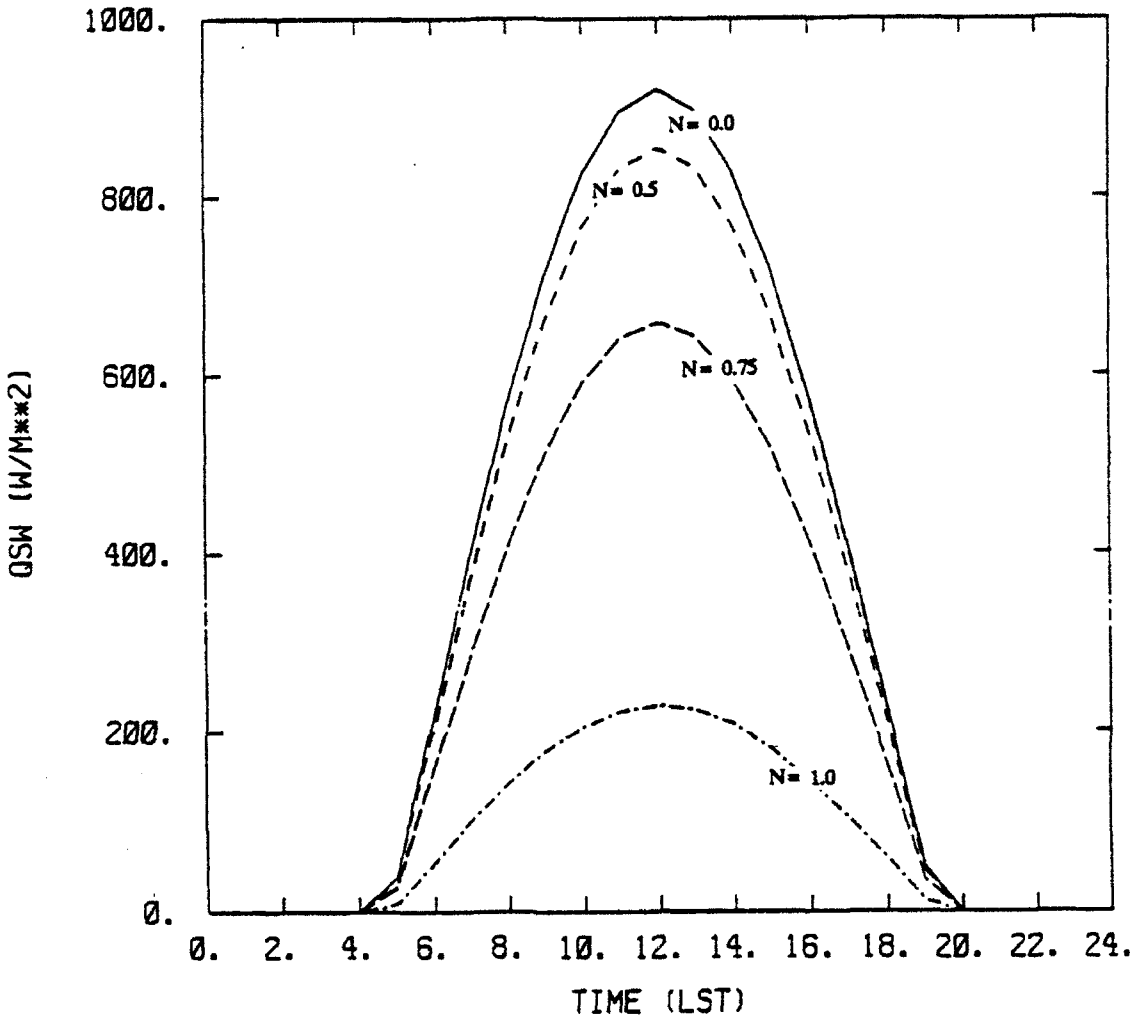

Figure 3a. Short-wave solar radiation, Q_{sw} predicted by Eqn. (4) as a function of time of day. Q_{sw} is shown for a latitude of 40°N and total cloud fractions, N, of 0.0, 0.5, 0.75, and 1.0 at the time of the summer solstice.

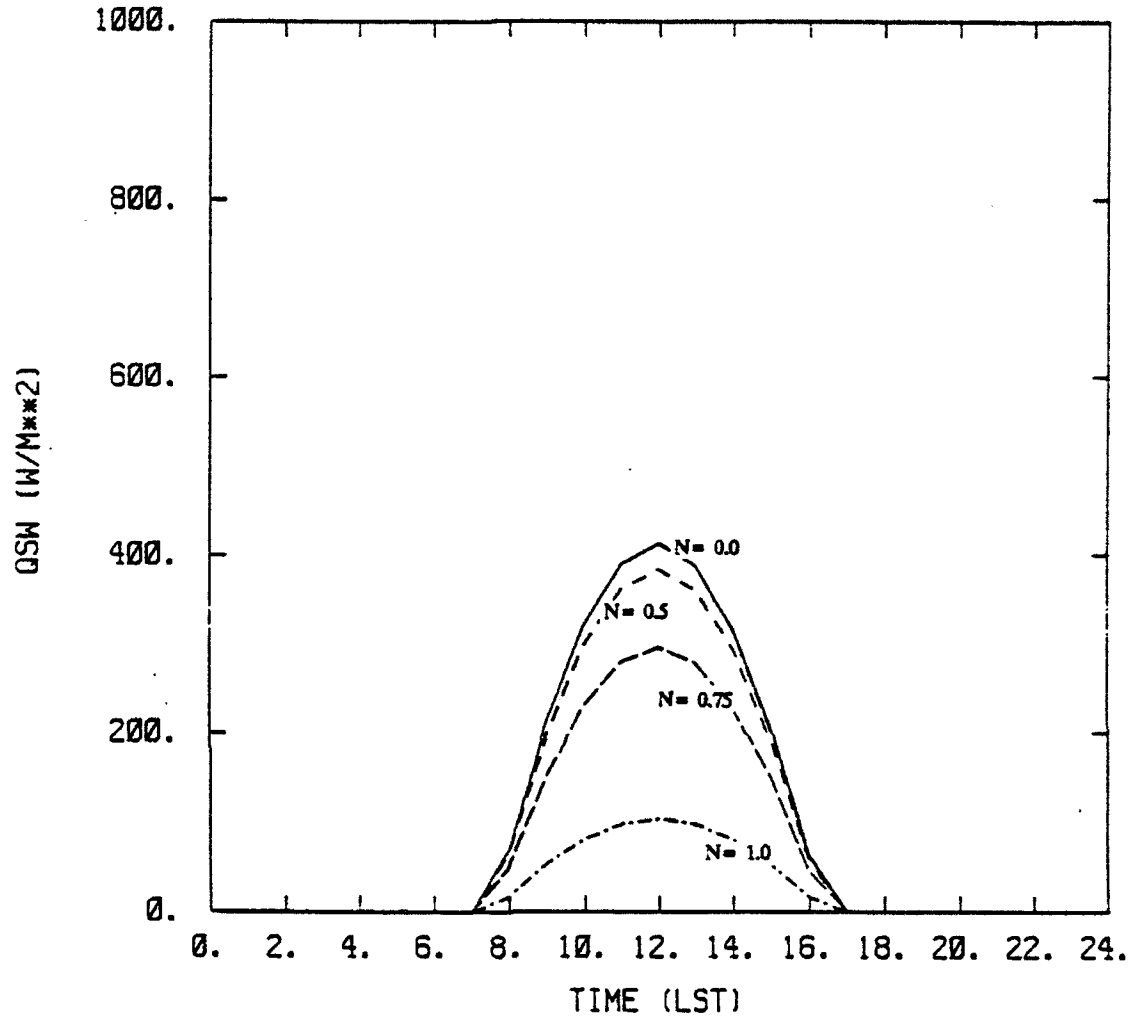

Figure 3b. Short-wave solar radiation, Q_{sw} predicted by Eqn. (4) as a function of time of day. Q_{sw} is shown for a latitude of 40°N and total cloud fractions, N, of 0.0, 0.5, 0.75, and 1.0 at the time of the winter solstice.

Table 3

Average Anthropogenic Heat Flux (Q_f) and Net Radiation (Q_*) for Several Urban Areas (From Oke, 1978)

Urban area/ latitude/ period	Population ($\times 10^6$)	Population density (persons/km^2)	Per capita energy usage ($MJ \times 10^3$/yr)	Q_f (W/m^2)	Q_* (W/m^2)
Manhattan (40°N)					
annual	1.7	28,810	128	117	93
summer				40	
winter				198	
Montreal (45°N)					
annual	1.1	14,102	221	99	52
summer				57	92
winter				153	13
Budapest (47°N)					
annual	1.3	11,500	118	43	46
summer				32	100
winter				51	-8
Sheffield (53°N)					
annual	0.5	10,420	58	19	56
West Berlin (52°N)					
annual	2.3	9,830	67	21	57
Vancouver (49°N)					
annual	0.6	5,360	112	19	57
summer				15	107
winter				23	6
Hong Kong (22°N)					
annual	3.9	3,730	34	4	~110
Singapore (1°N)					
annual	2.1	3,700	25	3	~110
Los Angeles (34°N)					
annual	7.0	2,000	331	21	108
Fairbanks (64°N)					
annual	0.03	810	740	19	18

heat input to the summertime value is nearly 5 in Manhattan, but only 1.5 in Vancouver, which has relatively mild winters. Hanna and Chang (1991) computed median values of 36 W/m^2 (summer) and 102 W/m^2 (winter) based on Oke's (1978) data.

Anthropogenic heating also shows considerable spatial variability. For example, in Greater London, McGoldrick (1980) found that Q_f varied from 0 to 5 W/m^2 in outer areas of the city, but exceeded 100 W/m^2 over several square kilometers in the center of the city (Landsberg, 1981). The maximum value averaged over one square kilometer was 234 W/m^2 (which is more than twice the average global solar radiation of 106 W/m^2). The spatial variability of the average annual anthropogenic heat flux for 2 km^2 grid cells in Tokyo is shown in Figure 4 (Kimura and Takahashi, 1991). The anthropogenic heat flux ranges from less than 10 W/m^2 over wide areas of the metropolitan area to over 100 W/m^2 in the inner core of the city.

Hanna and Chang (1991) point out the importance of the elevation of the anthropogenic energy release. For example, the heat input from a power plant occurs at an effective height of several hundred meters, while home heating and vehicle exhaust emissions are released near the surface. They note that only the near-surface components of anthropogenic heat flux should be considered in the computation of the surface energy balance.

These discussions point out that the anthropogenic heat input is significant, but that its magnitude and its spatial and temporal variability are rather uncertain. Consequently, it is difficult to parameterize. For example, suppose one wanted to model Minneapolis, which is not in Table 3. All one can say is that the average anthropogenic heat flux, Q_f, over the urban area is probably about 50 w/m^2, with an uncertainty of plus or minus a factor of two. The uncertainty would be multiplied by another factor of two or three if Q_f is estimated at a specific location, time of year, and hour of day. We recommend that local data on energy-use patterns be analyzed before making local estimates of Q_f for use in the surface energy balance equation.

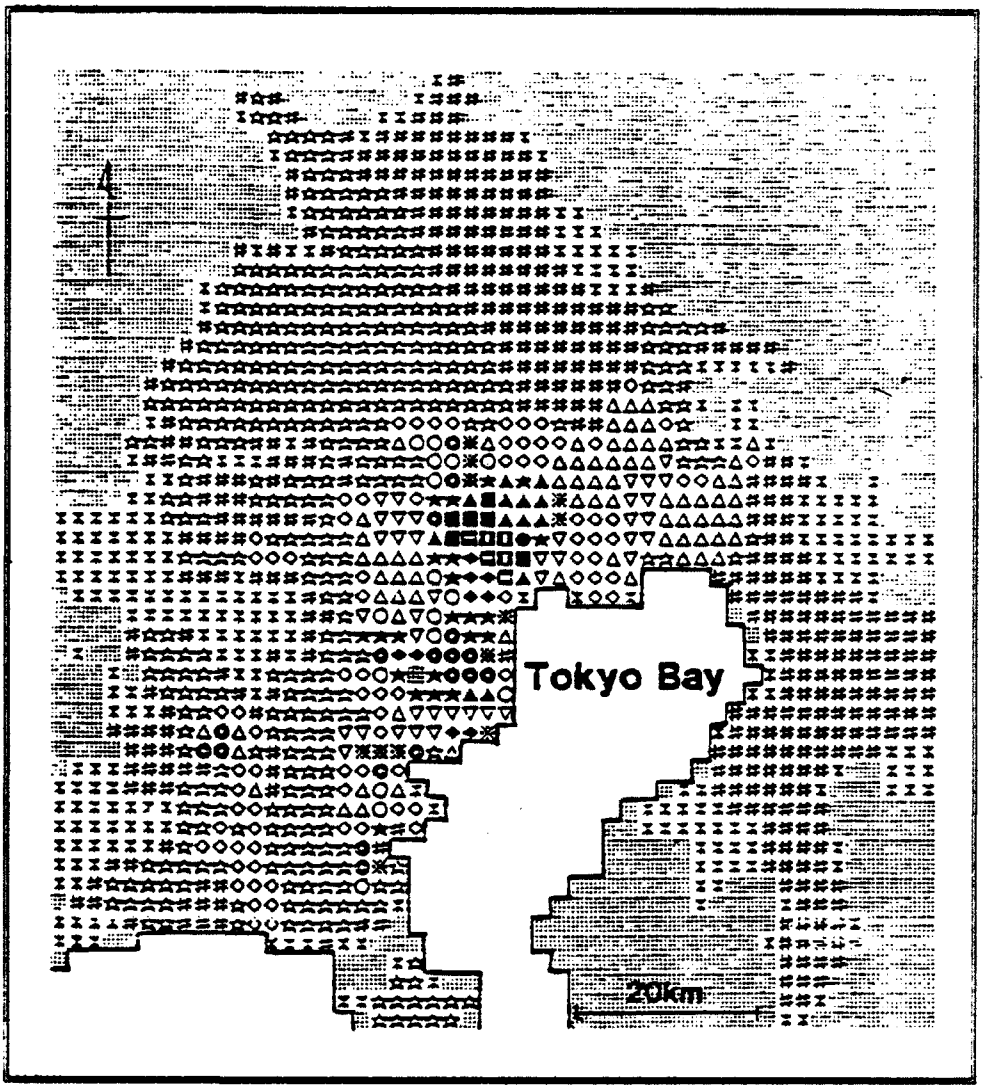

Figure 4. Average annual anthropogenic heat flux for 2 km square grid cells in the Tokyo Metropolitan area (From Kimura and Takahashi, 1991).

GROUND/STORAGE HEAT FLUX

The flux of heat into the ground or storage in surface materials, Q_g, is usually parameterized during the daytime as a fraction of the net radiation (e.g., DeBruin and Holtslag, 1982; Oke, 1978).

$$Q_g = c_g Q_* \tag{8}$$

where c_g is an empirical coefficient which depends on the properties of the surface. Holtslag and van Ulden (1983) obtained a value of c_g of 0.1 for a grass covered surface in the Netherlands. Oke (1982) indicates that typical ranges for c_g are 0.05 to 0.25 in rural areas, 0.20 to 0.25 in suburban areas, and 0.25 to 0.30 in urban regions and suggests that typical values of c_g are 0.15, 0.22, and 0.27 for rural, suburban, and urban areas, respectively. The larger values of c_g for urban area reflect the greater ability of building materials and pavement to transport heat (i.e., greater thermal conductivity, k) and the greater heat capacity, C, of some urban urban building materials. Oke (1982) suggests that the thermal admittance, $\mu=(kC)^{1/2}$ or thermal inertia is the most relevant measure of the thermal responsiveness of a surface. The greater thermal admittance of urban areas is expected to account for increased heat storage in cities, although direct measurements of Q_g on urban scales are difficult to make because of the variety of urban materials and complex geometry of the surface elements.

In some cases, the heat storage in the buildings can exceed the ground storage. However, when the buildings have significant size, the concept of a "surface" energy balance breaks down, and it is necessary to calculate the energy balance for a relatively deep layer extending from the building tops down to the ground surface. Lacking detailed measurements in this complex system, most modelers assume that the simple parameterizations described above are still valid approximations. These assumptions are probably reasonable during periods of strong solar insolation, but will tend to break down at night and during cloudy conditions, when the uncertainties in the energy fluxes are larger than the fluxes themselves (Hanna and Chang, 1992).

SENSIBLE AND LATENT HEAT FLUXES

One of the most important changes resulting from urbanization is the tendency for a shift in the partitioning of available energy during dry conditions from latent into sensible heat. This shift results from a number of factors, including decreased surface moisture availability in the urban area due to the hydrological characteristics its surface, higher urban surface temperatures, and less vegetation in the urban area. Measurements of urban sensible heat fluxes two to four times those in the surrounding rural areas are common (e.g., Godowitch et al., 1981; White et al., 1978; Hildebrand and Ackerman, 1984). Figure 5 plots observations of the net radiation, Q_*, and sensible heat flux, Q_h, for three sites in the St. Louis area which illustrates the increase in sensible heat with increased urbanization. Site 105 (urban commercial with little vegetation), Site 107 (urban residential with many trees), and Site 109 (rural agricultural). Also shown is the Bowen ratio, B, defined as the ratio of sensible to latent heat fluxes, i.e.,

$$B = \frac{Q_h}{Q_e} \qquad (9)$$

Oke (1978) gives the following typical values and ranges for the Bowen ratio:

Urban:	B = 1.5	(range 0.5 to over 4.0)
Suburban:	B = 1.0	(range 0.25 to 2.5)
Rural:	B = 0.5	(range 0.1 to 1.5)

During wet conditions, i.e., immediately following a rain event, the differences between urban and rural latent heat fluxes are much less as

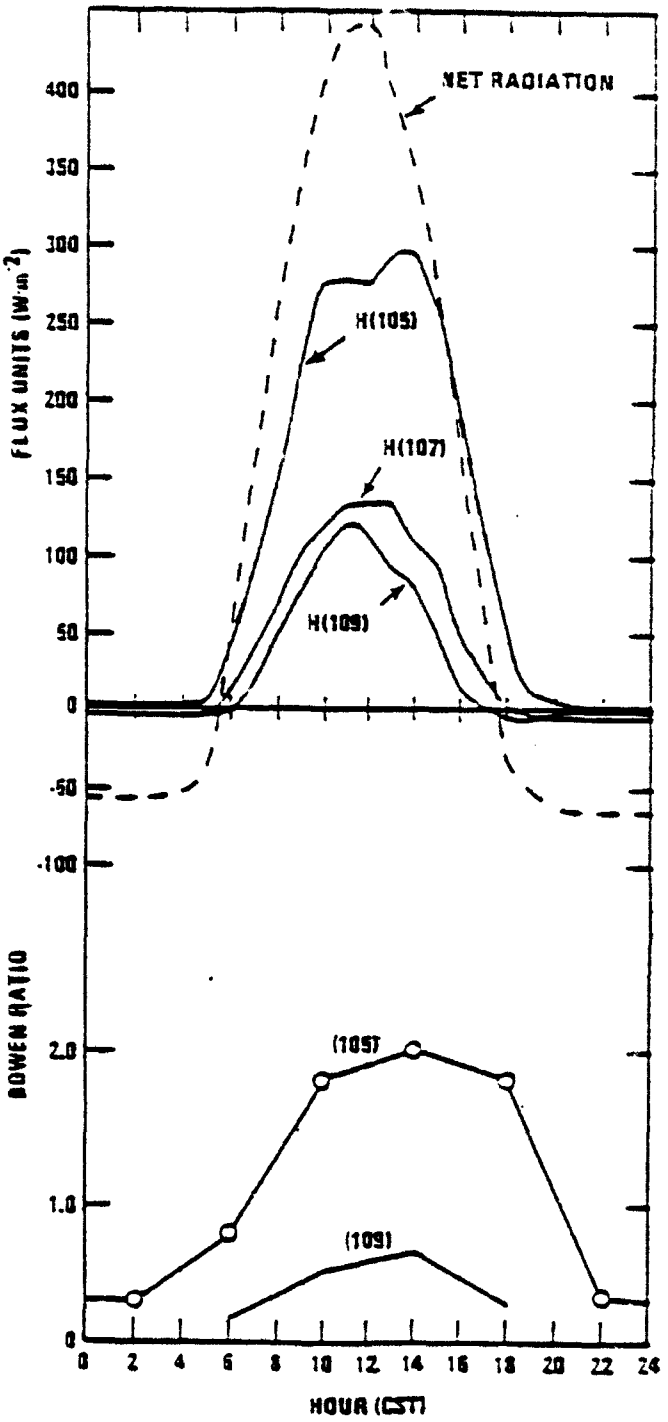

Figure 5. Diurnal variation of the sensible heat flux (H) at Sites 205 (urban commercial), 107 (urban residential), and 109 (rural agricultural) in the St. Louis area (top figure). Also shown is the net radiation at Site 105 (top figure) and the Bowen ratio for Sites 105 and 109. Data averaged over the month of August, 1976. (From Ching et al., 1978).

latent heat fluxes dominate due to evaporation from the wet surface. This is a reason for the considerable overlap in the ranges of Bowen ratio for the rural, suburban and urban areas. Also, the presence of irrigation systems (e.g., agricultural irrigation in rural areas or urban suburban lawn watering) can significantly affect the partitioning of latent and sensible heat over the affected areas.

Although some micrometeorological models allow specification of the Bowen ratio, which determines the relative magnitudes of the sensible and latent heat fluxes directly, Holtslag and van Ulden (1983) recommend a different technique based on a simplified version of the Penman-Monteith model. The Penman-Monteith expression for latent heat flux (neglecting anthropogenic heat flux) is given by van Ulden and Holtslag (1985) as:

$$Q_e = \frac{r\,S}{(1 + r\,S)}(Q_* - Q_g) + \frac{r\,\rho\,L}{(1 + r\,S)\,r_a}[q_s(T) - q] \qquad (10)$$

and

$$r = r_a/(r_a + r_s) \qquad (11)$$

$$r_a = (T - T_o)/(\theta_* u_*) \qquad (12)$$

and from deBruin and Holtslag (1982),

$$r_s = (S - B - 1)\,r_a + \frac{\rho\,L\,[q_s(T) - q]}{(Q_* - Q_g)} \qquad (13)$$

where r_a is the aerodynamic resistance to water vapor transfer from the surface to the air,

r_s is the surface resistance to water transfer from soil and vegetation to the surface,

q_s is the saturation specific humidity,

q is the actual specific humidity of the air,

L is the latent heat of vaporization,

T, T_o are the air and surface temperatures, respectively,

θ_* is the temperature scale for turbulence heat transfer, and

u_* is the surface friction velocity.

The first term of Eqn. (10) accounts for thermodynamic evaporation, or evaporation due to the presence of an external energy source (i.e., of strength $Q_* - Q_g$). The second term is called aerodynamic evaporation because it accounts for evaporation enhancement due to the flow of unsaturated air over the surface. Because some of the terms of the Penman-Monteith equation are difficult to evaluate operationally, van Ulden and Holtslag recommend the use of a simplified approximation to the expression (de Bruin and Holtslag, 1982; van Ulden and Holtslag, 1985) for latent heat flux referred to as the modified Priestley-Taylor model:

$$Q_e = \left[\frac{\alpha S}{S + 1} \right] (Q_* + Q_f - Q_g) + (\alpha)(\beta') \qquad (14)$$

where α is an empirical surface moisture parameter, and

β' is an empirical coefficient.

The basis for the Eqn. (14) is that there tends to be a strong correlation of both the thermodynamic and aerodynamic evaporation rates with the equilibrium evaporation, $Q_e(eq)$ (defined as the evaporation which would occur with a wet surface ($r_s = 0$) and saturated air ($q = q_s$). Thus, $Q_e(eq) = [S/(S+1)](Q_* - Q_g)$. This correlation is due to the fact that $(q_s - q)$ and $(Q_* - Q_g)$ exhibit similar diurnal patterns (e.g., see Figure 6). In Eqn. (14), the aerodynamic term is split into a portion correlated with $Q_e(eq)$ and an uncorrelated portion. The uncorrelated part is represented by the empirical constants $\alpha\beta'$. Holtslag and van Ulden (1983) found that $\beta' \approx 20$ W/m^2. A simple scheme for parameterizing the surface moisture parameter is discussed in more detail in the next section.

In Eqn. (14), the Q_f flux term has been added to the right side of Holtslag and van Ulden's equations to retain the generality of the equation for the urban case where anthropogenic heat fluxes may be significant. The term $\alpha\beta'$ results in positive latent heat fluxes during periods when the sensible heat flux is small but negative (e.g., around sunrise and sunset),

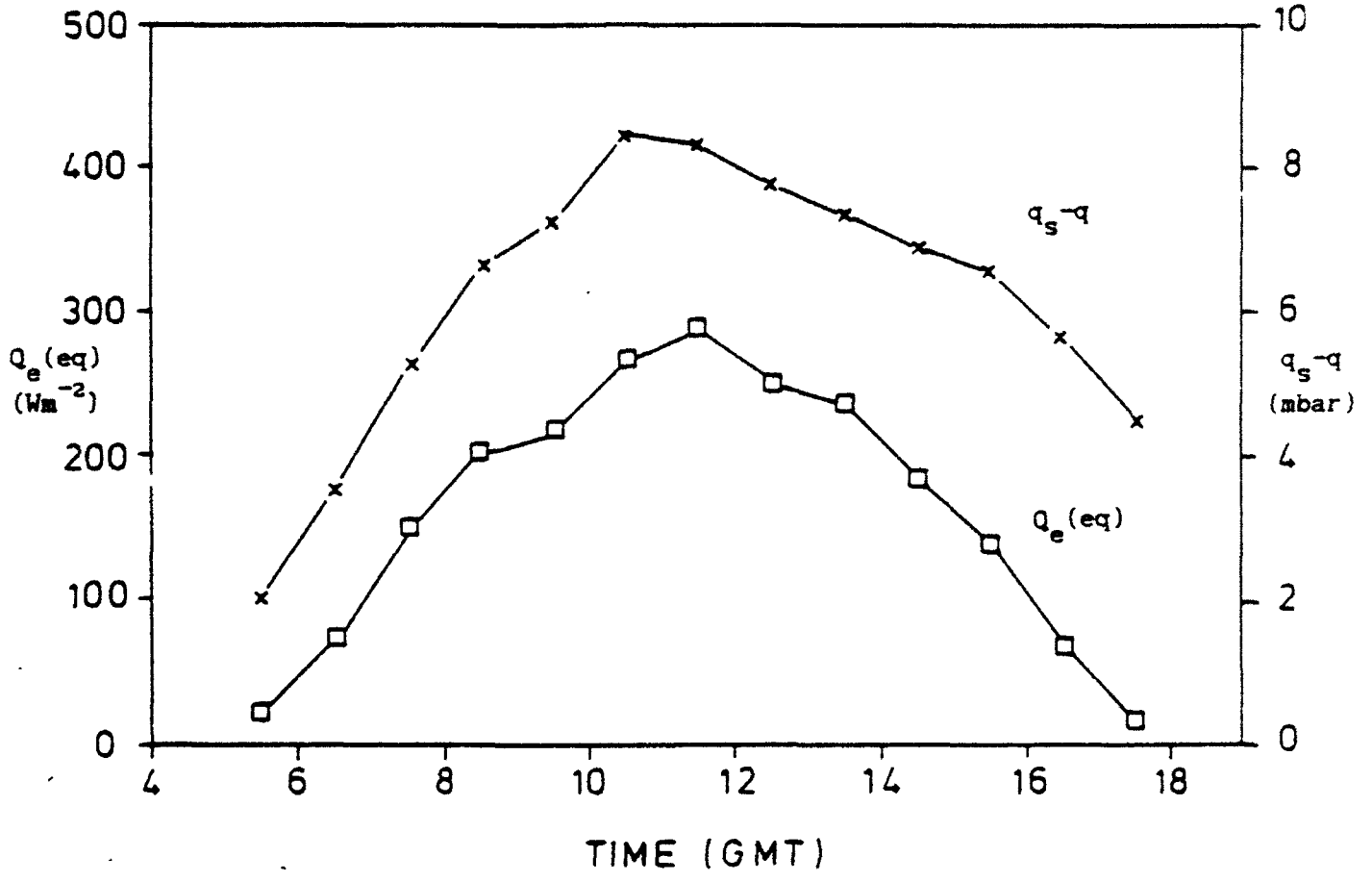

Figure 6. Diurnal variation of the water vapor deficit (q_s-q) and the equilibrium evaporation (Q_e(eq)). From de Bruin and Holtslag (1982).

which, as illustrated in Figure 7, is an observed feature of the behavior of sensible and latent heat fluxes (e.g., Oke, 1982; van Ulden and Holtslag, 1985).

The sensible heat flux, Q_h is determined by Holtslag and van Ulden (1983) as:

$$Q_h = \left[\frac{(1 - \alpha)(S) + 1}{S + 1} \right] (Q_* + Q_f - Q_g) - (\alpha)(\beta') \qquad (15)$$

2.3 Moisture Availability

Surface moisture availability is one of the key factors which determines the partitioning of available energy into sensible and latent heat, and thus, it has an important effect on atmospheric stability, turbulence levels, and dispersion rates. For example, Segal et al. (1990) found that a change in surface moisture from dry to wet conditions resulted in a one Pasquill stability class shift toward more neutral conditions around mid-day, and larger stability shifts in the morning and afternoon. They found consistently lower values of the ratio of convective velocity scale to wind speed (i.e., w_*/U), which is used as a measure of stability, with increases in soil moisture. Their study also found significantly lower mixing heights (by factors of 1.5 to 2.0) over wet surfaces.

The Holtslag and van Ulden model uses the surface moisture parameter, α, (sometimes called the Priestley-Taylor parameter) as a measure of moisture availability. The relationship between α and the Bowen ratio, B, can be obtained by combining Eqns. (14) and (15).

$$\alpha = \frac{[(S+1)/S]\ \Delta Q}{(1+B)\ \{\Delta Q + \beta'\ [(S+1)/S]\}} \qquad (16)$$

or, equivalently,

$$B = \frac{[(S+1)/S]\ \Delta Q}{\alpha\ \{\Delta Q + \beta'\ [(S+1)/S]\}} - 1 \qquad (17)$$

where $\Delta Q = Q_* + Q_f - Q_g$

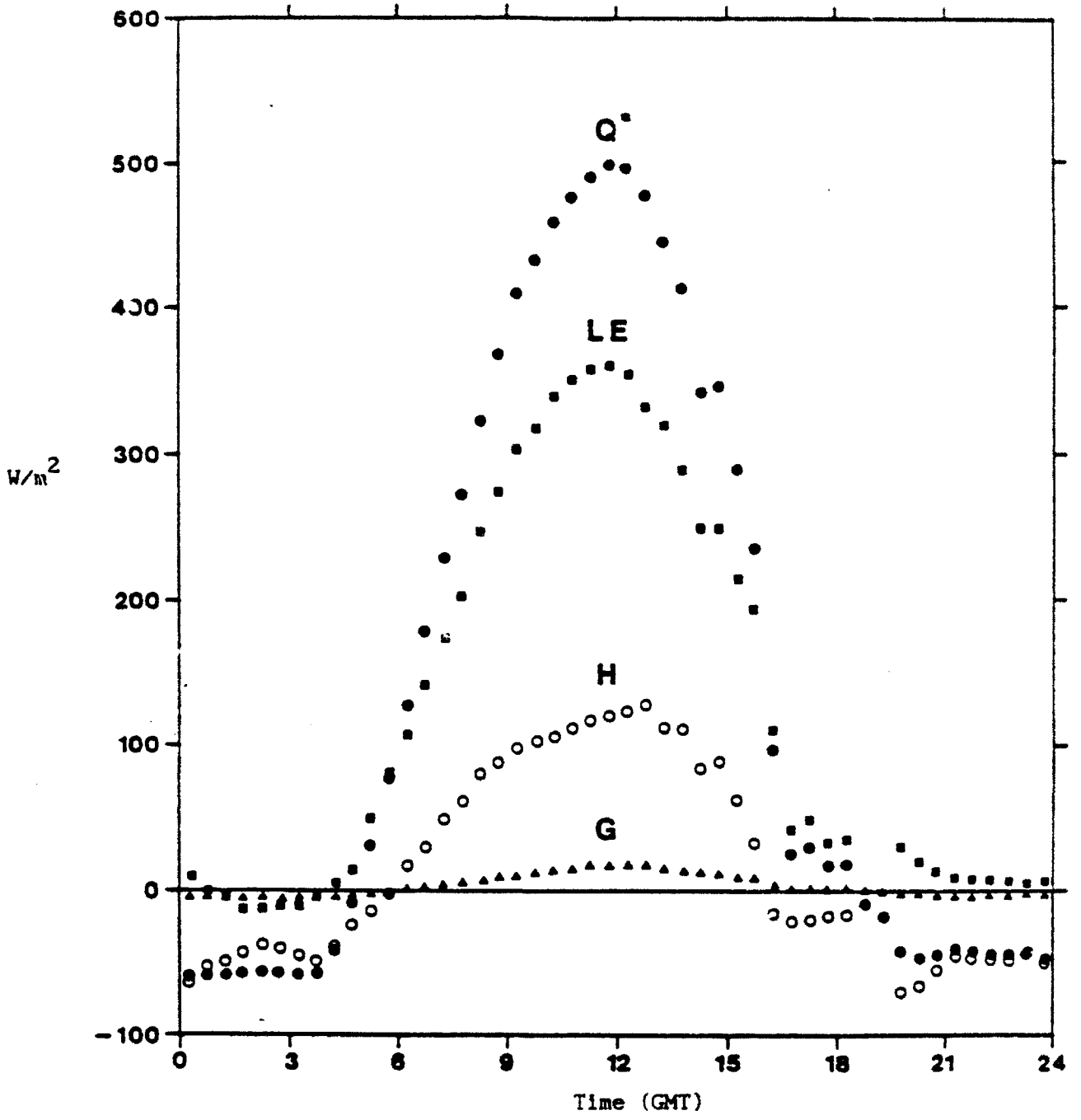

Figure 7. Diurnal variation of the components of the surface energy budget measured at a rural site in the Netherlands. Net radiation (Q^*), latent heat flux (LE), sensible heat flux (H), and soil heat flux (G). (From van Ulden and Holtslag, 1985).

Holtslag and van Ulden and others have applied the modified Priestley-Taylor approach over a variety of surfaces. Generally, these applications involved the specification of α as a constant over the length of the simulation. Typical values of α, based on empirical data of Holtslag and van Ulden and summarized by Hanna and Chang (1991) are:

$\alpha = 0.2$ (arid rural areas)
$\alpha = 0.5$ (urban areas, some parks, crops and fields during mid-summer when rain has not fallen for several days)
$\alpha = 0.8$ (crops, fields, or forest with sufficient moisture)
$\alpha = 1.0$ (normal wet grass in a moderate climate)

Two difficulties with this approach for the specification of α are (1) the qualitative nature of the descriptive relationship for α (e.g., "normal" wet grass, crops with "sufficient" moisture), and (2) the lack of time dependence to account for changes in α due to specific precipitation events or drying-out periods. As part of the current study, a simple scheme for predicting time-dependent surface moisture from routinely-available precipitation data and land use characteristics has been developed and is described in Section 2.2.2.

Figure 8 illustrates the relationship between the Bowen ratio and the surface moisture parameter at a temperature of 20°C for four values of ΔQ (i.e., 50, 100, 300, and 600 W/m^2). Typical values of the Bowen ratio for urban, suburban, and rural areas are 1.5, 1.0, and 0.5, respectively. Figure 7 indicates that these values of Bowen ratio correspond to values of α of approximately 0.55, 0.7, and 0.9, respectively, for typical mid-day values of ΔQ (i.e., 300 to 600 W/m^2). Thus, the values relating α to B with Eqn. (14) are consistent with typical empirical values of α suggested by de Bruín and Holtslag (1982), Holtslag and van Ulden (1983), and Hanna and Chang (1991). The typical value and range of Bowen ratio given by Oke (1978) and corresponding values of α as determined by Eqn. (16) with ΔQ = 300 to 600 W/m^2 are:

Urban: $B = 1.5$ (range 0.5 to over 4.0)
$\alpha = 0.55$ (range 0.2 to 0.9)

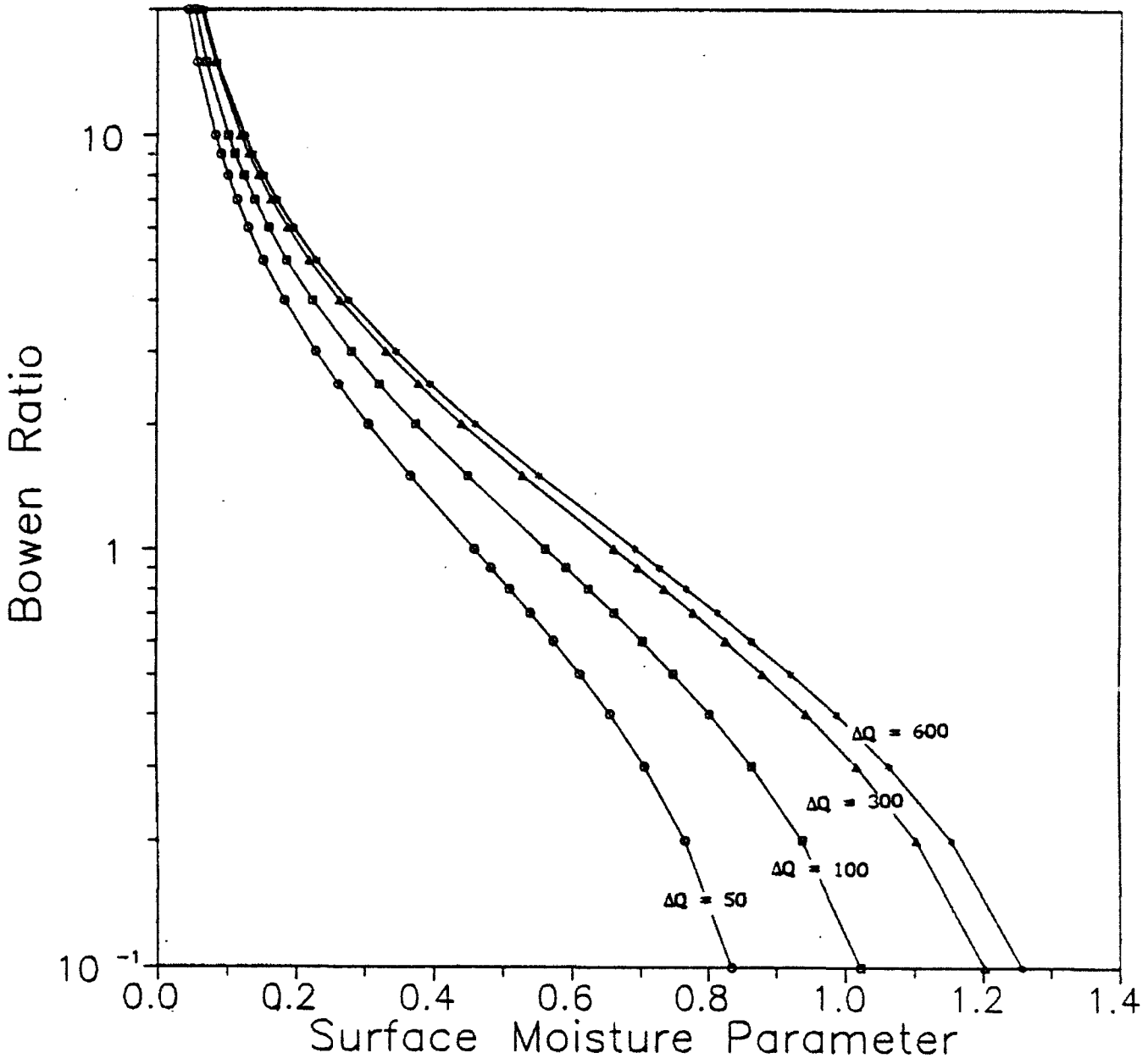

Figure 8. Plot of Bowen ratio, B, vs. the surface moisture parameter, α, as given by Eqn. (16) for T = 20°C, $\beta' \cong 20$ W/m^2, and ΔQ = 600, 300, 100, and 50 W/m^2.

Suburban: $B = 1.0$ (range 0.25 to 2.5)
$\alpha = 0.7$ (range 0.35 to 1.0)

Rural: $B = 0.5$ (range 0.10 to 1.5)
$\alpha = 0.9$ (range 0.55 to 1.2)

2.3.1 Soil Moisture - Numerical Models

Many coupled soil moisture-surface temperature numerical models have been developed to simulate sensible and latent heat fluxes from bare soil or vegetated surfaces. Although the complexity, high computational cost, and extensive data input requirements of these multi-layer prognostic models make them unsuitable for use in the current study, the results from the complex modeling studies are useful in understanding the behavior of soil moisture variability and can be helpful in developing simple parameterizations of the behavior of soil moisture.

Deardorff (1977) developed a model for evaporation over bare soil surfaces which included prognostic equations for soil moisture which distinguished between soil surface moisture and bulk soil moisture content. The evaporation rate is parameterized in terms of the surface volumetric water content, w_g, (reflecting conditions in the top few millimeters of the soil) rather than the bulk volumetric water content, w_b, (representing average volumetric soil moisture through a deeper layer from the surface down to about 50 cm).

$$E_g = \begin{cases} (w_g / w_{sat})\, E_{pot} & w_g \leq w_{sat} \\ E_{pot} & w_g > w_{sat} \end{cases} \qquad (18)$$

where w_{sat} is the soil-surface moisture content above which evaporation occurs at the potential rate ($w_{sat} \sim 0.75\, w_{max}$), and
E_{pot} is the potential evaporation rate.

Thus, the addition of moisture to the system when the surface moisture content is at or above $0.75\, w_{max}$ does not increase surface evaporation rate. In Deardorff's model, the surface moisture varies in response to the

difference in surface evaporation and precipitation and includes a term tending to exponentially restore surface moisture to the bulk value (w_b) in the absence of significant evaporation or precipitation. However, the model does not treat drainage from the thick (bulk) soil layer or runoff losses. In addition, because the bulk soil layer rather than the surface layer supplies the moisture for transpiration from vegetation, this parameterization is most appropriate for bare soil surfaces. However, Deardorff (1978) presents a generalized model which produces separate estimates for transpiration rates in vegetated areas and surface evaporation over areas without vegetation.

However, one of the significant results of the Deardorff (1977) model is the important effect of rapid soil surface drying on reducing the rate of evaporation. Rapid surface drying is expected to be important in urban environments, in which a large percentage of the surface is covered with impervious surfaces, and drainage systems exist to handle runoff. Figure 9 contains predicted values of w_g and w_b using Deardorff's model and observed values of w_g for a field of bare soil. The observed data is from Jackson (1973) for a field near Phoenix, Arizona during March 1971 for a seven day period following irrigation of the soil. Deardorff (1977) notes that the use of the bulk moisture content would have overpredicted evaporation rates by a factor between 1.5 and 5.6 during days 6 and 7.

Acs et al. (1991) developed a three-layer soil moisture and soil surface temperature model. The volumetric soil moisture content is based on the method of Sellers et al. (1986).

$$\frac{\partial w_1}{\partial t} = \frac{1}{D_1}\left(P - Q_{12} - \frac{1}{\rho_w} E \right) \tag{19}$$

$$\frac{\partial w_2}{\partial t} = \frac{1}{D_2}\left(Q_{12} - Q_{23} \right) \tag{20}$$

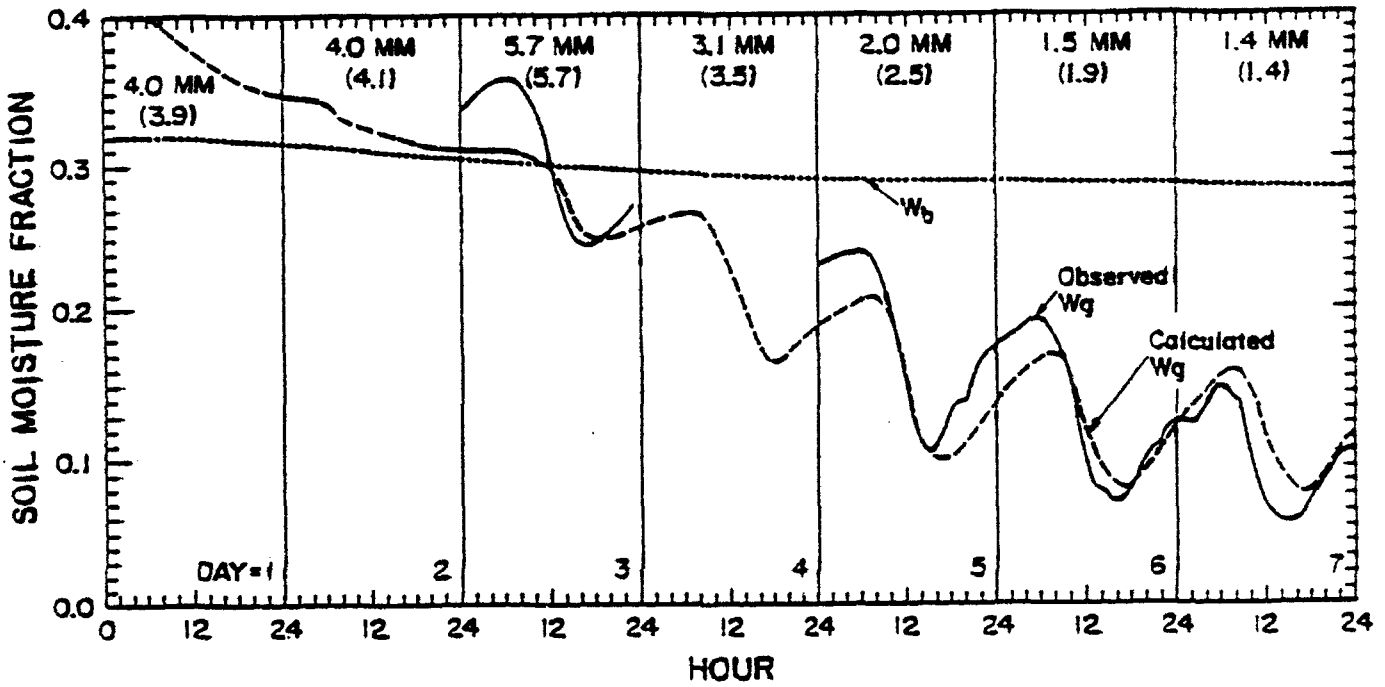

Figure 9. Predicted values of surface volumetric water content, w_g (dashed line), and bulk volumetric water content, w_b (dotted line). Also shown are observed values of w_g (solid line), predicted evaporation (mm) and observed evaporation (mm) in parentheses. (From Deardorff, 1977; observed data from Jackson, 1973).

$$\frac{\partial w_3}{\partial t} = \frac{1}{D_3}\left(Q_{23} - Q_3 \right) \qquad (21)$$

where w_i is the volumetric soil moisture of the ith layer,
P is the infiltration due to precipitation,
E is the soil surface evaporation rate,
D_i is the thickness of the ith soil layer,
ρ_w is the density of water,
$Q_{i,i+1}$ is the flow between soil layer i and i+1, and
Q_i is the drainage of water from the bottom of soil layer i.

The layers in Acs et al. (1991) model are 0-10 cm, 10-30 cm, and 30-60 cm in depth. Detailed information on the hydraulic properties of the soil, such as soil pore space and hydraulic conductivity at saturation, are used to compute the water flow between layers. The evaporation rate is assumed to be equal to the potential rate when w_1 exceeded 0.75 w_{sat}, where w_{sat} is the volumetric soil moisture at saturation, and a linear function of w_1 when w_1 is below 0.75 w_{sat}. Figure 10 illustrates the strong diurnal variation of soil moisture in the surface layer. Pronounced daytime drying is predicted along with increases in soil moisture during nighttime periods, although the model tends to overpredicted drying during the 5-day periods.

Pan and Mahrt (1987) investigated the interactions among soil moisture, energy fluxes, and boundary layer development. They used a detailed 34-layer atmospheric boundary layer model (extending up to 4 km in height) coupled with a two-layer soil model (5 cm deep top layer, 95 cm deep bottom layer) in the study. They describe three stages of soil drying with different effects on energy fluxes and boundary layer development. These stages are illustrated in Figure 11. In the first stage, surface evaporation is at the potential rate and is determined primarily by wind speed, relative humidity, and incoming solar radiation. Surface evaporation is strong, which limits surface heating and therefore boundary layer development. The potential and actual evaporation rates decrease moderately with time due to a gradually moistening of the boundary layer.

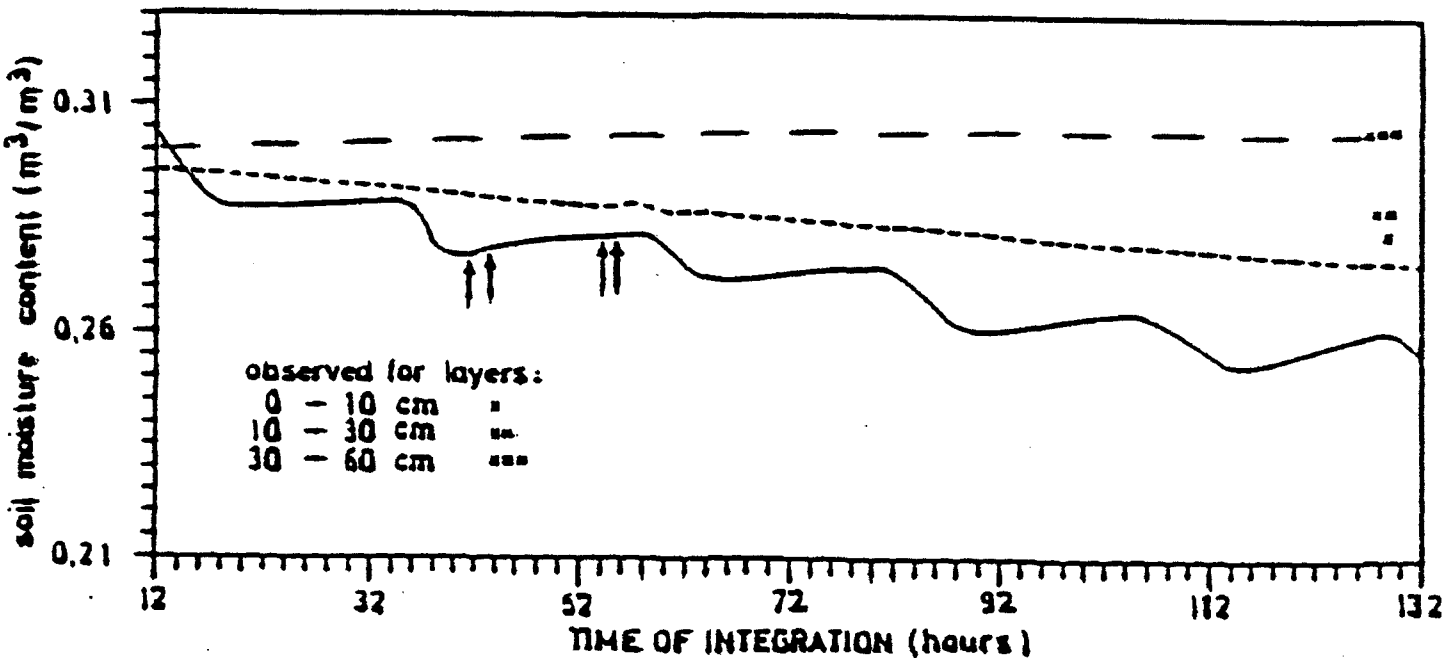

Figure 10. Predicted soil moisture in three layers [0-10 cm (solid line), 10-30 cm (fine dashed line), and 30-60 cm (coarse dashed line)]. Periods with precipitation are indicated with arrows. Data for a surface of bare soil during 15-20 April, 1988. (From Acs et al., 1991).

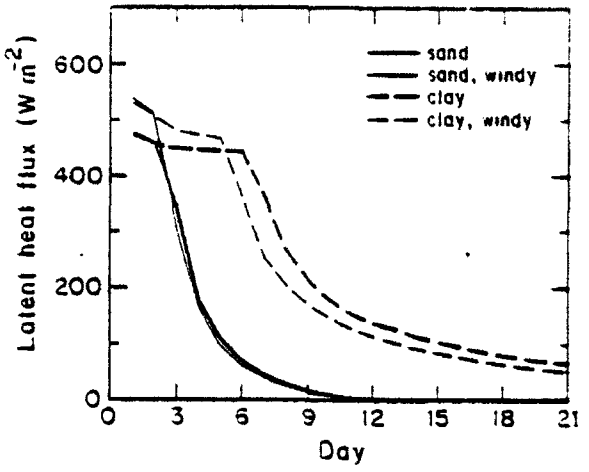

(a)

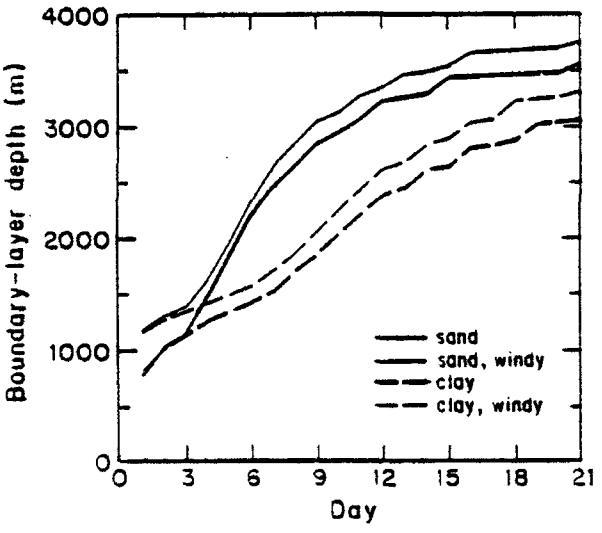

(b)

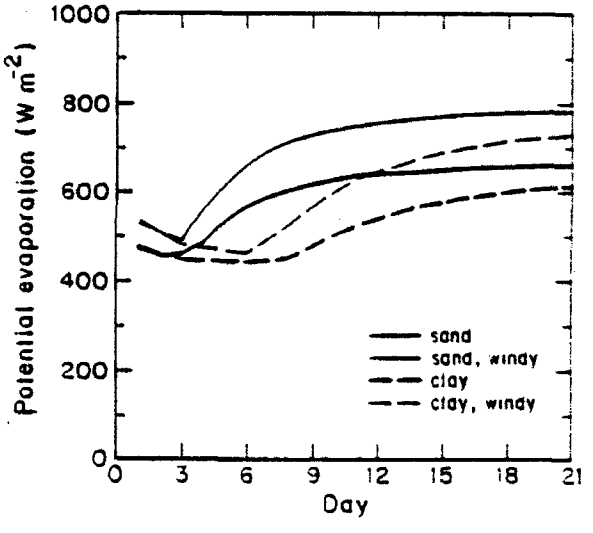

(c)

Figure 11. Predicted evolution of (a) noontime surface latent heat flux (W/m^2), (b) noontime boundary layer height, and (c) noontime potential evaporation for two surface types (clay and sand) during periods of moderate geostrophic winds (5 m/s) and strong geostrophic winds (10 m/s) on the summer solstice. (From Pan and Mahrt, 1991).

In the second stage, the evaporation rate decreases rapidly below potential evaporation values due to drying of the surface layer (Figure 11(a)). Actual evaporation is limited by the rate of soil moisture transport to the surface, which is determined by soil properties and the moisture gradient within the soil. With a lower surface evaporation rate, surface temperature, sensible heat flux and boundary layer height all increase significantly (Figure 11(b)). In the second stage, the entrainment of drier air from above the boundary layer can be significant, even exceeding the surface evaporation, and leading to an overall drying of the boundary layer. Even though potential evaporation increases due to higher temperatures and boundary layer drying (Figure 11(c)), the actual evaporation rate decreases due to limited surface moisture availability.

The final stage of drying occurs near steady-state conditions are reached. Eventually the mid-day surface evaporation rate decreases to a small fraction of the potential rate (i.e., < 10%). The soil moisture is significantly depleted and changes further only slowly. The boundary layer development is deep, and is characterized by warm and dry conditions.

Pan and Mahrt (1987) conducted sensitivity tests of the modeling results on factors such as vegetation and solar radiation. Vegetation tends to reduce the differences between the three stages. Because vegetation draws moisture from a deeper layer (i.e., the root zone), soil drying occurs more slowly and the onset and magnitude of the stage 2 effect is reduced (see Figure 12(a)). Reduced solar radiation lowers the potential evaporation rate which also slows the drying process. At wintertime levels of solar radiation, the vertical transport of soil moisture from deeper soil layers during nighttime periods can restore or nearly restore the surface moisture level sufficiently to maintain daytime potential evaporation rates (see Figure 12(b)).

Noilhan and Planton (1989) used a force restore method based on Deardorff (1977, 1978) to parameterize surface moisture and its effect on latent and sensible heat fluxes. The volumetric soil moisture content is described by:

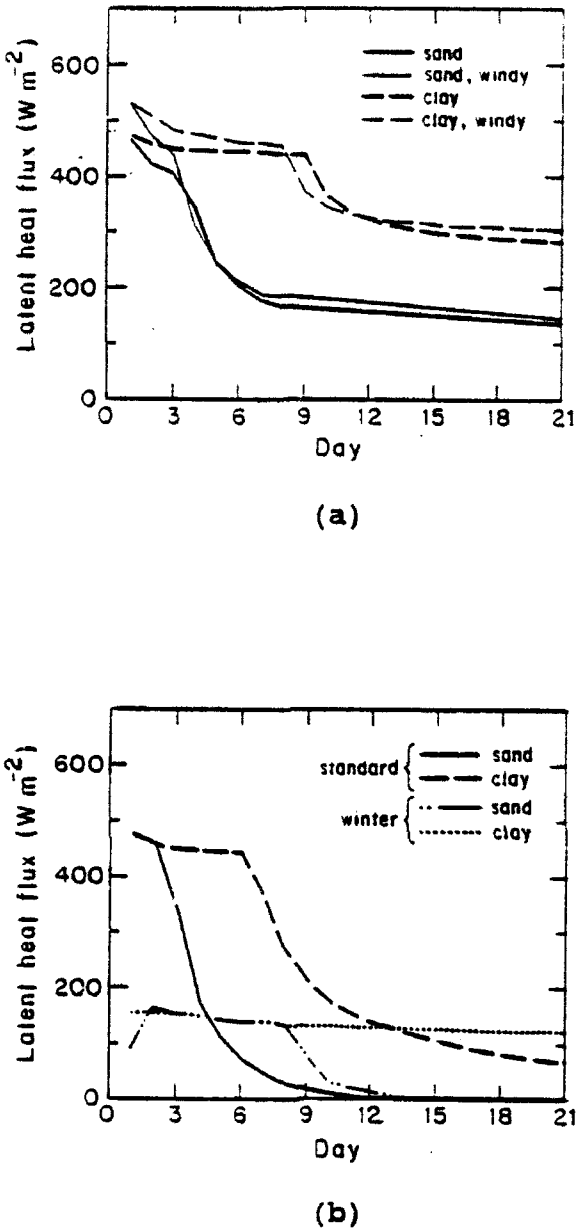

Figure 12. Results of sensitivity tests showing (a) noontime surface latent heat flux (W/m^2) for a vegetated surface on the summer solstice, and (b) noontime surface latent heat flux (W/m^2) for a bare surface on the winter solstice. (From Pan and Mahrt, 1991).

$$\frac{\partial w_g}{\partial t} = \frac{C_1}{\rho_w d_1}(P - E) - \frac{C_2}{\tau}(w_g - w_{geq}) \qquad (22)$$

$$0 < w_g \leq w_{sat}$$

$$\frac{\partial w_2}{\partial t} = \frac{1}{\rho_w d_2}(P - E - E_{tr}) \qquad (23)$$

$$0 < w_2 \leq w_{sat}$$

where w_g is the volumetric soil moisture content in a thin surface soil layer (few millimeters in depth),

w_2 is the average volumetric soil moisture content through a deeper layer from the surface down to a depth d_2 (~ 50 cm),

w_{geq} is the equilibrium surface volumetric soil moisture content when gravity balances the capillarity forces,

E_{tr} is the transpiration rate,

τ is a time constant,

d_1 is a normalization constant (~ 10 cm), and,

C_1, C_2 are empirical coefficients.

The other variables have been defined previously. In their model, the atmospheric conditions forcing the system (i.e., solar radiation wind speed, specific humidity, temperature) are specified rather than computed. The most important improvements of Deardorff's model made by Noilhan and Planton (1989) are (1) a correction to Deardorff's restore term in Eqn. (22) to account for gravitational effects (i.e., the use of w_{geq} instead of w_2 in the last term of the equation) and (2) calibration of the coefficients in the equation based for different types and soil wetness values.

2.3.2 Soil Moisture - Capacitance Model

A simple capacitance model has been developed to allow the soil moisture parameter, α, to be estimated operationally from routinely-available precipitation data and land use information. The model is intended to

reproduce some of the most significant features of the behavior of the comprehensive soil moisture-surface evaporation models discussed in the previous section, but with significantly more modest input and computational requirements.

The model consists of two capacitors: a slow-response capacitor to simulate bulk moisture content through a deep layer and a fast-response capacitor to respond to moisture variations in a thin surface layer. Precipitation acts to "charge" the capacitor and evaporation "discharges" the system. Feedback is allowed between the bulk and surface moisture parameters to simulate a build-up ("re-charge") of surface moisture due to transport from deeper layers during periods of low evaporation (e.g., see Figure 9). Different values of the capacitor's time constant are used to parameterize the variable responses to moisture input of different surface (land use) types (e.g., urban, suburban, agricultural, vegetated surfaces). In converting the "charge" (q) to a soil moisture parameter (α), a cap is applied to α which results in a nearly constant evaporation rate in the initial (stage 1) phase of drying from a moist surface, followed by a period of rapid decrease in evaporation (i.e., the stage 2 effect), and finally, very low, near steady-state evaporation rates characteristic of stage 3 (see Figure 11(a))

During drying-out periods, the state of charge of a capacitor is:

$$q(t+\Delta t) = q(\min) + \Delta q \exp\left\{ \frac{-(t_v + \Delta t)}{\tau} \right\} \qquad (24)$$

$$\Delta q = q(\max) - q(\min) \qquad (25)$$

where q is the "charge" of the system at time $(t+\Delta t)$,

$q(\min)$, $q(\max)$ are minimum and maximum values of q for a particular land use type,

τ is a time constant at time $(t+\Delta t)$ which depends on land use type and time of day, and,

t_v is a virtual time computed from q at the previous time step (i.e., $q(t)$).

The time constant and minimum/maximum values of q must be determined empirically. Additional work, beyond the scope of the current study, is required to develop tables of "typical" values of these parameters as a function of routinely-available data, such as land use. However, because the system is likely to be heavily driven by the measured precipitation history, it is expected that the results will not be overly sensitive to errors in the specification of the empirical parameters τ, q(min), and q(max).

It is necessary to compute a virtual time, t_v, because τ may vary from one time step to the next. Therefore, t_v is computed to reflect the previous state of the system in terms of the new τ at time $t+\Delta t$.

$$t_v = -\tau \ln \left\{ \frac{q(t) - q(min)}{\Delta q} \right\} \qquad (26)$$

When the system is being recharged (i.e., during a precipitation event), the state of the system is:

$$q(t+\Delta t) = q(min) + \Delta q \left\{ 1 - \exp \left[\frac{-(t_v + \Delta t)}{\tau} \right] \right\} \qquad (27)$$

where the virtual time is:

$$t_v = -\tau \ln \left\{ 1 - \frac{q(t) - q(min)}{\Delta q} \right\} \qquad (28)$$

The time constant during precipitation periods is computed from the precipitation amount:

$$\tau = \xi / R \qquad (29)$$

where ξ is an empirical parameter (hour/mm) which depends on the surface type, and,
R is the precipitation amount (mm).

The surface soil moisture parameter, α, is estimated from the capacitor charge, q, as:

$$\alpha = \begin{cases} q & q < 1.0 \\ 1.0 & q \geq 1.0 \end{cases} \qquad (30)$$

Thus, the addition of moisture to the system when it is at or beyond fully moist conditions does not change the soil moisture parameter or the surface evaporation rate. Also, the surface evaporation rate will remain nearly constant during the initial phase (i.e., stage 1) of a drying-out period until q drops below a value of one. However, q (and α) will vary rapidly with continued drying once q decreases to be less than one (i.e., stage 2). Further drying will result in q approaching a constant value of q(min) (i.e., stage 3).

In the capacitance model used in this study, two values of q are tracked: q_f is the value for the fast-response capacitor representing moisture in a thin surface layer and q_s is the value for the slow-response capacitor (tracking bulk moisture content). Each capacitor has its own value of ξ and τ (i.e., ξ_f, ξ_s and τ_f, τ_s) reflecting the different rates of response to precipitation input and evaporation output. Additional capacitors with slower response time simulating deeper (or thicker) layers could be added. However, the two-capacitor model is used to demonstrate the technique and appears to be adequate. Although τ is a function of the evaporation rate, no attempt has been made to compute hourly values for the current set of tests, although this could be a future enhancement. However, different values of τ have been used for daytime and nighttime periods to reflect the large differences in evaporation rates between these periods.

During nighttime periods when evaporation rates are low, the surface moisture content tends to be restored toward the bulk value due to moisture transport from deeper layers to the surface. If the nighttime surface moisture is greater than the bulk value, the surface moisture will tend to slowly decrease and approach the bulk value from above. These features of the soil moisture behavior are reproduced by setting $q(min) = q_s$ (if $q_f > q_s$) and $q(max) = q_s$ (if $q_f < q_s$).

The daytime drying and nighttime restoring of the surface moisture predicted by the capacitance model is shown in Figure 13 for a seven-day drying period. The assumed values for the model parameters are

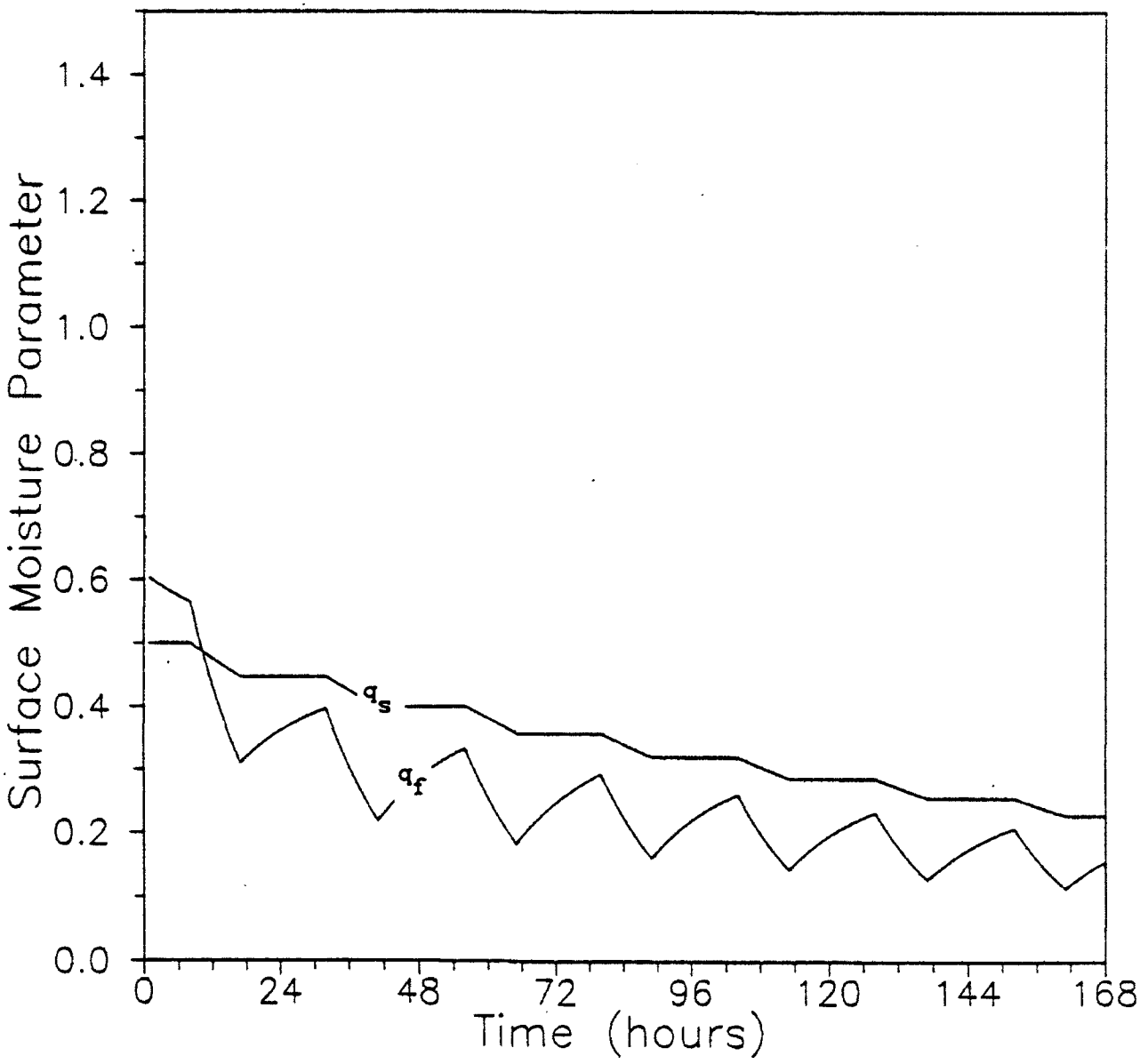

Figure 13. Illustration of daytime drying and nighttime moistening of surface soil as predicted by the capacitance model for a seven-day drying out period. Fast-response (surface layer) value (q_f) and slow-response (bulk layer) value (q_s) of soil moisture are plotted. Model parameters are τ_f(day) = τ_f(night) = 15 hr, τ_s(day) = 80 hr, and τ_s(night) = 99999 hr.

τ_f(day) = τ_f(night) = 15 hr, τ_s(day) = 80 hr, and τ_s(night) = 99999 hr. The predicted surface moisture cycle shown in Figure 13 can be qualitatively compared to the observed behavior shown in Deardorff (1977) for Days 3 and 5-7 (Figure 9).

The capacitance model has been used estimate soil moisture for the base-case conditions described in the 21-day simulation of a drying-out period by Pan and Mahrt (1991). The soil moisture is predicted with the capacitance model for two surface types (sand and clay) using the following assumed model parameters:

clay:	τ_s(day) = 65 hrs	sand:	τ_s(day) = 20 hrs
	τ_s(night) = 99999 hrs		τ_s(night) = 99999 hrs

Assuming noontime conditions of ΔQ = 600 W/m^2, T = 25°C, and β'=20 W/m^2, and using Eqn. (14), the latent heat flux (in W/m^2) can be expressed as:

$$Q_e \text{ (noon)} = 464\ \alpha \qquad (31)$$

where, α is determined using Eqn. (30) with $q=q_s$. Figure 14 shows the predicted noontime latent heat flux using soil moisture predicted by the capacitance model along with the predictions from the numerical model of Pan and Mahrt (1991). The capacitance model successfully reproduces the main features of the more complex model for both surface types. Each of the three stages of evaporation discussed above can be seen in the predictions of both models.

The relationship between α and q depends on the type of surface being modeled. For example, as found by Deardorff (1977) and (1978), evaporation from a bare soil surface is determined by surface moisture content. However, over a vegetated surface, moisture from the deeper (bulk) layer controls evapotranspiration. Therefore, in that case, α is most appropriately related to q_s. In our testing of the model for an urban environment, a short time scale was assigned to τ_f to allow q_f to represent moisture on the surface of the urban surfaces (e.g., wet pavement, wet ground surfaces). The time scale for τ_s was selected to reflect longer term average urban moisture conditions.

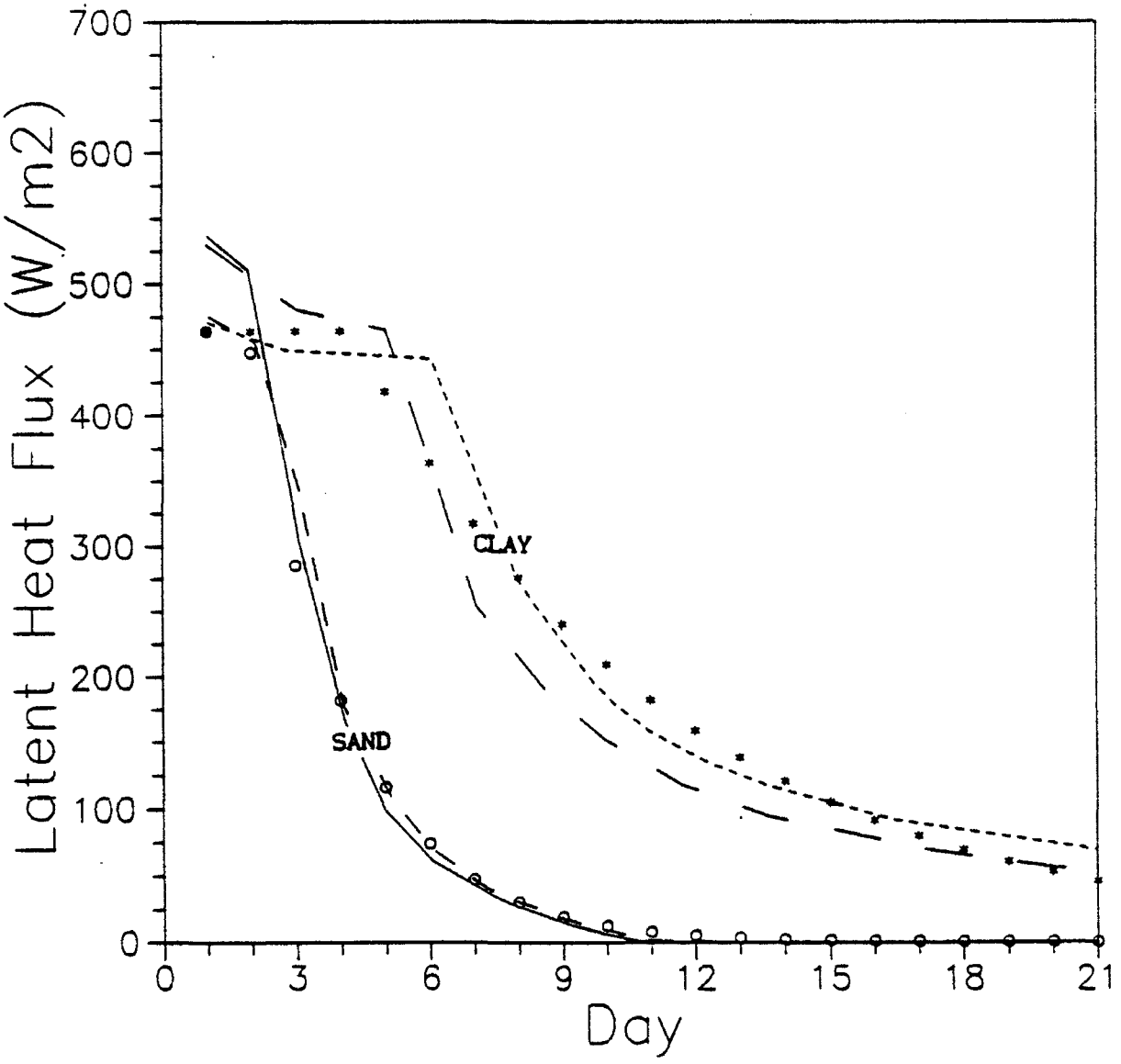

Figure 14. Predicted noontime surface latent heat flux (W/m^2) based on soil moisture predictions of capacitance model for clay soil (*) and sandy soil (o) for a 21-day drying out period. Also shown are the numerical model predictions of Pan and Mahrt (1991): clay (short dash), clay, windy conditions (long dash), sand (intermediate dash), sand, wind conditions (solid).

The moisture parameter α was determined by applying Eqn. (30) to the larger of q_f or q_s. Thus, α increases rapidly with the occurrence of precipitation as the urban surfaces become wet, but relatively quickly returns to its longer term value determined by q_s after the surface moisture evaporates.

As an illustration of the capacitance model technique, predicted values of q for a three month period are plotted in Figure 15(a) and 16(a) for an urban area and vegetated rural area, respectively. Daily precipitation values for Boston, Massachusetts during the period from May through July, 1989 were used in both simulations (see Figure 15(b)). Monthly total precipitation for May and June were near climatological mean values (89.9 mm and 72.1 mm, respectively, representing deviations from normal of +0.5 mm and -2.0 mm). Precipitation for July (129.3 mm) was above normal by 61.2 mm.

The two-capacitor moisture model was run for 92 days starting on May 1 with an initial value of q of 0.5 for both areas. The main difference in the urban/rural inputs assumed were the values of ξ_s (96 hr/mm (urban) vs. 48 hr/mm (rural)) and τ_s (24 hr (urban) vs. 96 hour (rural)). The larger value of ξ_s for the urban area reflects the diversion of a fraction of the precipitation from soil storage in the urban environment by impervious surfaces, urban drainage systems and runoff. Thus, a given amount of precipitation in an urban area will produce a smaller change in the bulk soil moisture content than in a rural area where more of the precipitation is absorbed into the ground. Similarly, values of τ_s were selected to allow a more rapid drying of the urban area. Unlike the rural environment, where the precipitation makes its way into surface and deeper soil layers and therefore is available to be evaporated over the next few days, much of the precipitation input into the urban system is carried away, resulting in a more rapid return to normal dry conditions. Similar values of τ_f (12 hrs (urban), 15 hrs (rural)) and ξ_f (24 hr/mm for both) were used in the simulations.

The predictions of the capacitance model in Figure 15(a) are generally consistent with observations of the Bowen ratio (related to α by Eqn. (16)) as described in Section 2.2. Typical observed urban values of the Bowen ratio are ~ 1.5, which corresponds to a mid-day α of ~ 0.5. (According to Eqn. (30), α=q when $q < 1.0$, and $\alpha = 1.0$ when $q \geq 1.0$). The predicted daily

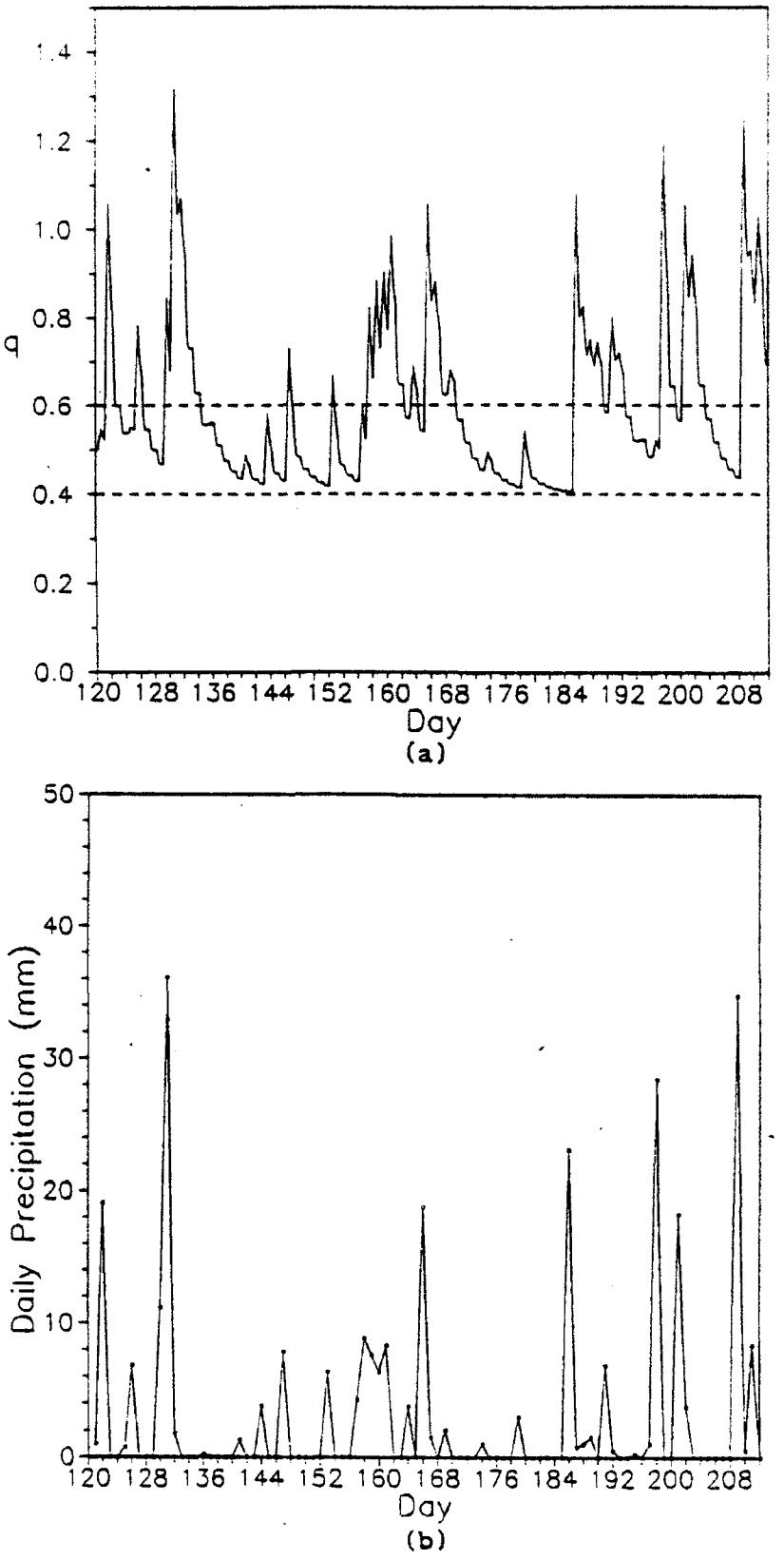

Figure 15. (a) Predicted values of q using typical urban values of the capacitance model inputs and Boston precipitation for May, June, and July 1989.

(b) Daily precipitation totals (mm/day) for the same time period.

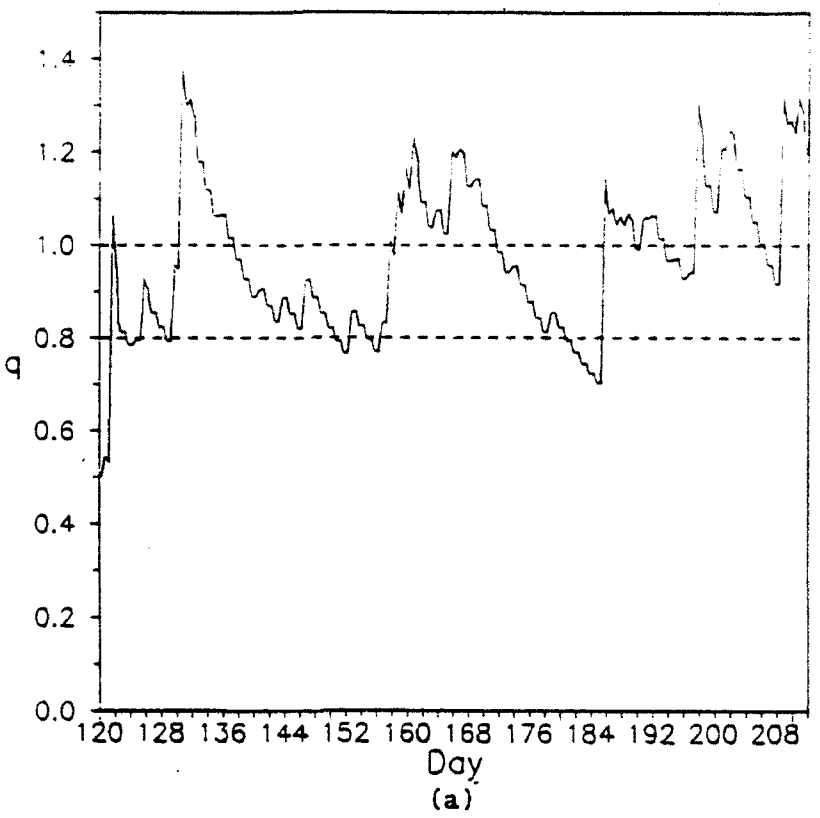

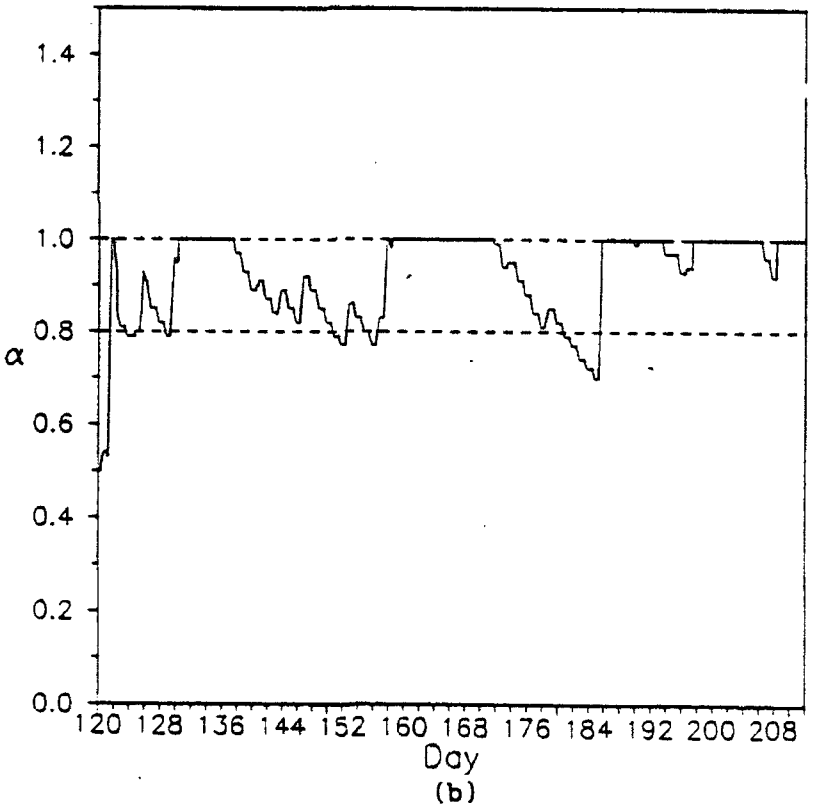

Figure 16. (a) Predicted values of q using typical rural values of the capacitance model inputs. The Boston precipitation values (see Fig. 15b) for May-July, 1989 were used. (b) Corresponding values of the soil moisture parameter (α).

averaged urban value of α for most of the days without precipitation are in the range 0.4 to 0.6 (i.e., on 40 of 55 dry days) with an average dry day value of 0.5. During precipitation events, q (and α) increase rapidly as a result of precipitation wetting of the urban surface. However, α also falls quickly after the precipitation event, reflecting rapid drying of the urban environment. In Figure 16(b), the soil moisture parameter in the rural area stays within the range 0.8 to 1.0 for most of the period. These values of α are consistent with observed rural Bowen ratios ~ 0.5. During a six-day period with no precipitation in late June and early July, drying results in a drop in α to 0.68. Also note that the low initial value of α = 0.5 is quickly adjusted by the model to more typical rural values.

The results discussed in this section suggest that the capacitance model may be a useful tool in estimating the time variability of the soil moisture parameter, which is one of the key inputs to the energy balance model. The capacitance model produces reasonable values of α for both urban and rural environments. It requires as input only routinely-available precipitation data and empirical time scale parameters (i.e., τ and ξ) which can be related to land use. The test case simulations produce estimates of soil moisture which are consistent with observations of typical Bowen ratios in urban and rural areas.

2.4 Parameterization of Boundary Layer Parameters

A number of meteorological preprocessors have been developed which employ an energy balance method based on Holtslag and van Ulden (1983) to estimate the sensible heat flux from routinely available meteorological data and then compute boundary layer parameters such as the surface friction velocity and Monin-Obukhov Length with empirical or iterative schemes. Such preprocessors include METPRO (Hanna et al., 1986), SIGMET (Scire and Wojichowski, 1987), SIGPRO (Hanna and Chang, 1990 and 1992) and CALMET (Scire et al., 1990a), as well as several others. Of these, all except METPRO contain features which allow them to be used in urban areas. However, because SIGPRO has several enhanced features and has the advantage of being recently evaluated using data from urban field experiments in St. Louis and Indianapolis, it is recommended as the starting point for the Phase II study.

SIGPRO uses the sensible heat flux, Q_h, produced from the energy balance model (see Section 2.2) along with observations of the wind speed, u, and estimates of the surface roughness length, z_o, and displacement height, d, to compute the following boundary layer parameters:

u_* - surface friction velocity $[(-\overline{u'w'})^{1/2}]$,
L - Monin-Obukhov length,
h - mixing height, and,
w_* - convective velocity scale

Because SIGMET allows the input of hourly values of the surface moisture parameter, α, it can be easily coupled to the capacitance soil moisture model described in Section 2.3.2.

2.4.1 Friction Velocity and Monin-Obukhov Length

The friction velocity is expressed in terms of the following wind profile formula:

$$u = \frac{u_*}{k} \left\{ \ln \left(\frac{z - d}{z_o} \right) - \psi_m(z/L) \right\} \qquad (32)$$

where u is the wind speed at height z,
k is the von Karman constant (~0.4),
z_o is the surface roughness length, and,
ψ_m is an universal stability correction factor which is a function of z/L (e.g., Dyer and Hicks, 1970).

Hanna and Chang (1992) recommend the following rules of thumb for d and z_o: $d \sim 0.5h_r$ and $z_o \sim 0.1h_r$, where h_r is the height of roughness elements (Stull, 1988). The Monin-Obukhov length is defined as:

$$L = \frac{- u_*^3 \, T \, \rho \, c_p}{k \, g \, Q_h} \qquad (33)$$

where T is the air temperature,

ρ is the air density,

c_p is the specific heat at constant pressure, and,

g is the acceleration due to gravity.

If the buoyancy effects of water vapor are to be included, Q_h in Eqn. (33) is replaced with the virtual heat flux, Q_{hv}, and T is replaced with the virtual temperature, T_v, as described in Section 2.4.2.

NEUTRAL CONDITIONS

Under neutral conditions, ψ_m is zero, and u_* can be computed directly from Eqn. (32), i.e.,

$$u_{*n} = \frac{ku}{\ln[(z-d)/z_o]} \tag{34}$$

Once u_* is known and Q_h is determined from the energy balance equations, L is computed directly from its definition (Eqn. (33)).

UNSTABLE CONDITIONS

When ψ_m is not zero, solution of Eqns. (32) and (33) requires the application of a computationally demanding iterative technique. An alternative approach used in SIGPRO and SIGMET for unstable conditions is an empirical relationship developed by Wang and Chen (1980) which can be solved analytically.

$$u_* = \frac{ku}{\ln[(z-d)/z_o]}\left[1 + d_1 \ln(1 + d_2 d_3)\right] \tag{35}$$

where

$$d_1 = 0.128 + 0.005\ln(z_o/z) \quad \text{if } z_o/z \leq 0.01 \tag{36}$$

$$= 0.107 \quad \text{if } z_o/z > 0.01 \tag{37}$$

$$d_2 = 1.95 + 32.6(z_o/z)^{0.45} \tag{38}$$

$$d_3 = \frac{Q_h}{\rho c_p} \frac{kgz}{Tu_{*n}^3} \tag{39}$$

The term $d_1 \ln(1 + d_2 d_3)$ represents the correction due to instability and u_{*n} is defined in Eqn (34).

Hanna and Chang (1990, 1992) tested the analytical formula against values produced by the iterative solution of u_* and L. They found that the Wang and Chen (1980) expression produced values within 10% of the results determined by the iterative solution for z = 10 m, d = 0, z_o = 1 m, and a large value of Q_h (400 W/m^2). Better agreement was found for smaller roughness elements and smaller sensible heat fluxes. In addition, the analytical solution was computationally significantly faster. Therefore, Hanna and Chang (1990) recommend the use of the Wang and Chen (1980) approach.

Again, once u_* and Q_h are known, L is computed directly from Eqn. (33).

STABLE CONDITIONS

The Weil and Brower (1983) method for estimating u_* is applied in SIGPRO during stable conditions. A first estimate of the scaling temperature, θ_*, is calculated using Holtslag and Van Ulden's (1983) equation:

$$\theta_{*1} = 0.09(1 - 0.5N^2) \tag{40}$$

where N is the total cloud cover in fractions, and θ_* has units of °K. Another estimate of θ_* is made from the profile equation for temperature:

$$\theta_{*2} = \frac{TC_{dn}u^2}{18.8zg} \tag{41}$$

where the neutral drag coefficient C_{dn} is defined as $k/\ell n[(z - d)/z_o]$.

Then, θ_* is set equal to the smaller of θ_{*1} and θ_{*2}.

The sensible heat flux, Q_h, is defined during stable conditions as:

$$Q_h = - \rho c_p u_* \theta_* , \tag{42}$$

For large values of u (or u_*), θ_{*1} (which depends only on cloud cover) is smaller than θ_{*2}, but an additional check on the product $u_*\theta_*$ must be made, since Q_h does not keep increasing indefinitely with higher wind speeds. In SIGPRO, the value of θ_* is not allowed to exceed $0.05/u_*$, where the numerator has units of °K m/s and denominator has units of m/sec. This limit is estimated from observations of heat fluxes during high-wind, stable conditions.

The friction velocity, u_*, can be calculated from:

$$u_* = \frac{C_{dn} u}{2} \left[1 + \left[1 - \left(\frac{2u_o}{C_{dn}^{1/2} u} \right)^2 \right]^{1/2} \right] \tag{43}$$

where $u_o = \left(4.7 z g \theta_* / T \right)^{1/2}$.

Because θ_* is set equal to the smaller of θ_{*1} and θ_{*2}, the following condition is always met:

$$\frac{2u_o}{C_{dn}^{1/2} u} \leq 1 \tag{44}$$

During stable conditions, SIGPRO enforces a lower limit on L in recognition of the fact that the atmosphere is less stable over urban areas than over rural surfaces. The minimum values of L used as default values in SIGPRO are based on the observation that the mechanical mixed layer is about 2 to 3 times the typical building height (Uno et al., 1988) and that L represents the height of the mechanically mixed layer. Hanna and Chang (1990) suggest the values in Table 4 for use for the various land use categories defined in the Auer (1978) scheme.

Table 4

Minimum Values of Monin-Obukhov Length
During Stable Conditions
for Various Land Use Types
(From Hanna and Chang, 1990)

Auer (1978)	Class	Description	Minimum L
C1	Commercial	> 40 story buildings	150 m
		10-40 story buildings	100 m
		< 10 story buildings	50 m
I1, I2	Industrial		50 m
R3	Compact Residential		50 m
R1, R2	Residential		25 m
A	Agricultural		2 m

2.4.2 Inclusion of Buoyancy Effects of Water Vapor

During most conditions over land surfaces, evaporation rates are sufficiently small that the buoyancy effects of water vapor are negligible in the expressions for the boundary layer parameters. However, evaporation rates can sometimes be high enough (e.g., after a summertime precipitation event with high net radiation conditions) that water vapor can affect the density stratification near the surface. The effects of water vapor buoyancy can be accounted for by using a virtual heat flux, Q_{hv} instead of Q_h and a virtual temperature (T_v) instead of T in the relevant equations for L (Eqn. (33)) and w_* (Eqn. (50)). Arya (1988) suggests the following formula to estimate Q_{hv}:

$$Q_{hv} = Q_h + 0.61\ c_p\ \Theta\ Q_e/L_e \qquad (45)$$

where Θ is the mean potential temperature,
c_p is the specific heat at constant pressure (10^3 J/(kg K)),
L_e is the latent heat of evaporation (2.5×10^6 J/kg), and,
Q_e is the latent heat flux.

The virtual temperature is the temperature of dry air having the same density as moist air at the same pressure. It is approximated as:

$$T_v \sim T\ (1 + 0.6\ q_m) \qquad (46)$$

where q_m is the mixing ratio ($q_m = RH\ q_s/100.$),
RH is the relative humidity of the air, and
q_s is the saturation mixing ratio (temperature and pressure dependent).

If the data to compute T_v is not available, its effect can be neglected, since the most important effect of water vapor buoyancy on L is accounted for in the Q_{hv} term. Arya (1988) notes that T_v usually does not vary from T by more than a few degrees, so $g/T_v \sim g/T$. However, Q_{hv} can sometimes be significantly larger than Q_h. For example, at Θ = 280 K, Eqn. (45) yields $Q_{hv} \sim Q_h + 0.07\ Q_e$ or equivalently $Q_{hv} \sim Q_h(1 + 0.07/B)$, where B is the Bowen ratio. Since the Bowen ratio can reach values as low as 0.1, under these conditions Q_{hv} is increased by 70% over Q_h.

2.4.3 Mixing Height

The convective boundary layer (CBL) is assumed to be capped by a relatively thin interfacial layer separating it from the stable air aloft. Stable air is entrained into the interfacial layer as a result of vertical mixing due to thermals penetrating the top of the CBL. Within the mixed layer ($0.1h < z < h$), the potential temperature θ and wind speed u are relatively uniform, but in the interfacial layer, they rapidly adjust with height to their values in the overlying stable air.

Carson (1973) has simplified the modeling of boundary layer evolution by ignoring radiation, latent heat effects, and advection of energy. He includes the effects of 1) time-dependent surface heating; 2) capping layer stability; 3) large-scale air subsidence; and 4) a uniform distribution of θ with z within the CBL, a step change $\Delta\theta_h$ at the top of the CBL ($z = h$), and a linear variation with z in the overlying stable air. Carson also assumes that the stable air is composed of as many as three vertical layers, each with a different lapse rate, instead of a single stable layer.

Weil and Brower (1983) modified Carson's model by:

- permitting the elevated stable layer to have an arbitrary temperature distribution with z (i.e., an infinite number of vertical layers);
- accounting for surface stress-induced (mechanical) mixing, which can be important at night and in the early morning hours when the heat flux is low or zero; and
- neglecting subsidence.

Convective and mechanical mixing are assumed to be independent of one another, so that when one of these mixing modes is operative, the other is not. Figure 17 shows an example of an assumed potential temperature distribution, where the solid curve is the initial temperature profile, $\theta_s(z)$, and the dashed curve is the idealized profile at a later time t. The

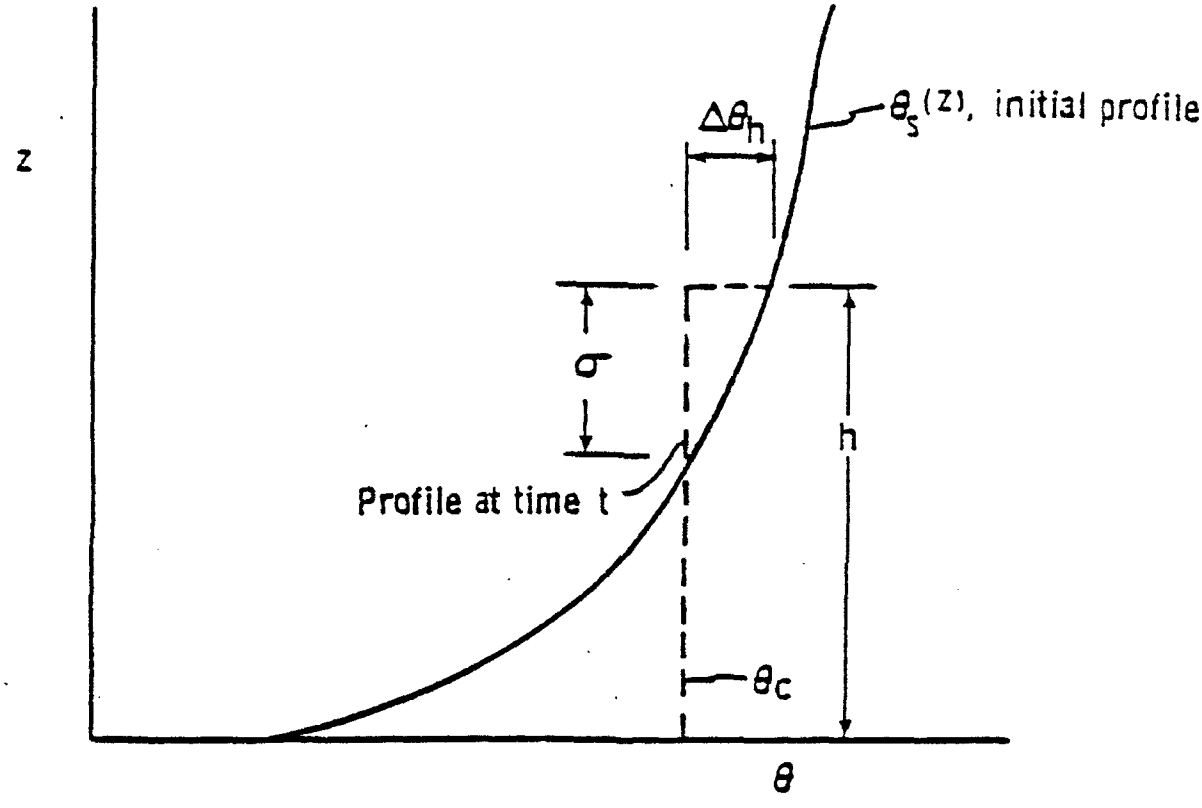

Figure 17. Mixing height computation using the modified Carson method. (From Hanna and Chang, 1990).

"overshoot" σ is a measure of the degree of entrainment or interfacial mixing and is a function of time, as are the mixed-layer temperature and height, θ_c and h, respectively, and the temperature jump $\Delta\theta_h$. When there is no overshoot, $\Delta\theta_h = 0$, and the mixed-layer only "encroaches" on the elevated stable layer.

The growth of the *convective* mixing height is assumed to be controlled by the bombardment of the stable lid by thermals originating at the surface. Computationally, the incremental (hourly) change of the area under the temperature profile curve (see Figure 17) is proportional to the hourly surface heat flux, and the area under the temperature profile θ_s curve is proportional to the accumulated surface heat flux. Thus, the area under the temperature profile curve at time t is given by the formula:

$$h\theta_s(h) - \int_o^h \theta_s dz = (1 + 2A) \int_o^t \frac{Q_h(\tau)}{\rho c_p} d\tau \qquad (47)$$

where Q_h is the surface heat flux, W/m^2,
ρ is the air density,
c_p is the specific heat of air at constant pressure, and
A is the proportionality constant (ration of heat flux at the top of boundary layer to that at the surface), taken as 0.2 after Deardorff (1980).

Weil and Brower's formulation of the *mechanical* mixing height, after Tennekes (1973) and Kato and Phillips (1969), is similar to Eqn. (47) except that the right side of the equation is a function of the friction velocity u_*:

$$h^2 \theta_s(h) - 2 \int_o^h z\theta_s dz = 2 \frac{BT_o}{g} \int_o^t u_*^3(\tau) d\tau \qquad (48)$$

where T_o is the surface temperature and B is a constant (~ 0.5).

For each hour, the higher of the mechanical or convective mixing height is chosen. This method does not use surface temperature explicitly (unlike the other methods), and therefore avoids inconsistencies between the on-site temperature and the off-site upper sounding temperature at 12Z.

The interpolation scheme developed by Nieuwstadt (1981) for the calculation of the nocturnal boundary layer height (h) is used in SIGPRO:

$$h = (L/3.8)\ [-1+(1+2.28\ u_*/fL)^{1/2}] \qquad (49)$$

where

f is the Coriolis parameter, $= 2\Omega \sin\phi$;
Ω is the angular speed of rotation of the earth, $= 7.292 \times 10^{-5}$ rad s^{-1}; and
ϕ is the latitude.

The solution for h given by this formula approaches $0.4(u_*L/f)^{1/2}$ for small L, as suggested by Zilitinkevich (1972), and approaches $0.3u_*/f$ for large L (the solution for neutral conditions).

2.4.4 Convective Velocity Scale

In the convective boundary layer, the appropriate velocity scale is w_*, which can be computed directly from its definition using previously defined estimates of Q_h and h:

$$w_* = \left(\frac{g\ Q_h\ h}{T\ \rho\ c_p}\right)^{1/3} \qquad (50)$$

If water vapor buoyancy effects are important, Q_h should be replaced with Q_{hv} and T replaced with T_v in Eqn. (50), as described in Section 2.4.2.

3. URBAN DISPERSION AND STABILITY

3.1 Stability Classification

Most dispersion models use the Pasquill stability classification method (Pasquill, 1961) or a variation (e.g., Turner, 1964) to define atmospheric stability and dispersion rates. The Pasquill scheme contains six discrete stability classes ranging from extremely unstable (class A) to moderately stable (class F). The Pasquill class is determined based on wind speed, solar radiation, and cloudiness. Solar radiation is categorized as strong, moderate, or slight (see Table 5).

The Turner (1964) scheme is widely used in current EPA dispersion models. It includes a modification for a seventh category (extremely stable - class 7) and distinguishes between low overcast and high overcast conditions before assigning the neutral stability category. The relationship between Turner's classes 1-7 and Pasquill's classes A-F are (Gifford, 1976; Hanna et al., 1982): A=1, B=2, C=3, D=4 and 5, E=6, and F=7.

Golder (1972) developed a nomogram related the surface roughness length and inverse Monin-Obukhov length to the Pasquill stability classes. The Golder nomogram is shown in Figure 18. Various empirical equations have been fit to Golder's graph relating L to z_o as a function of stability class, including equations by Shir and Shieh (1974) and Irwin (1979a). The Irwin equation was based on a power law relationship:

$$L^{-1} = a\,(z_o)^b \qquad (51)$$

where the coefficients a and b are shown in Table 6.

Lui et al. (1976) developed an empirical expression relating Monin-Obukhov length to surface roughness and a stability parameter, P (Pasquill A $\longrightarrow$ P = -3, Pasquill B $\longrightarrow$ P = -2, ..., Pasquill F $\longrightarrow$ P = +2), such that

Table 5

The Pasquill (1961) Stability Categories

10-m wind speed (m/s)	Insolation			Night	
	Strong	Moderate	Slight	Thinly overcast or > 4/8 low cloud	< 3/8 cloud
< 2	A	A-B	B	F	F
2-3	A-B	B	C	E	F
3-5	B	B-C	C	D	E
5-6	C	C-D	D	D	D
> 6	C	D	D	D	D

Neutral (D) category assumed for overcast conditions, day or night.

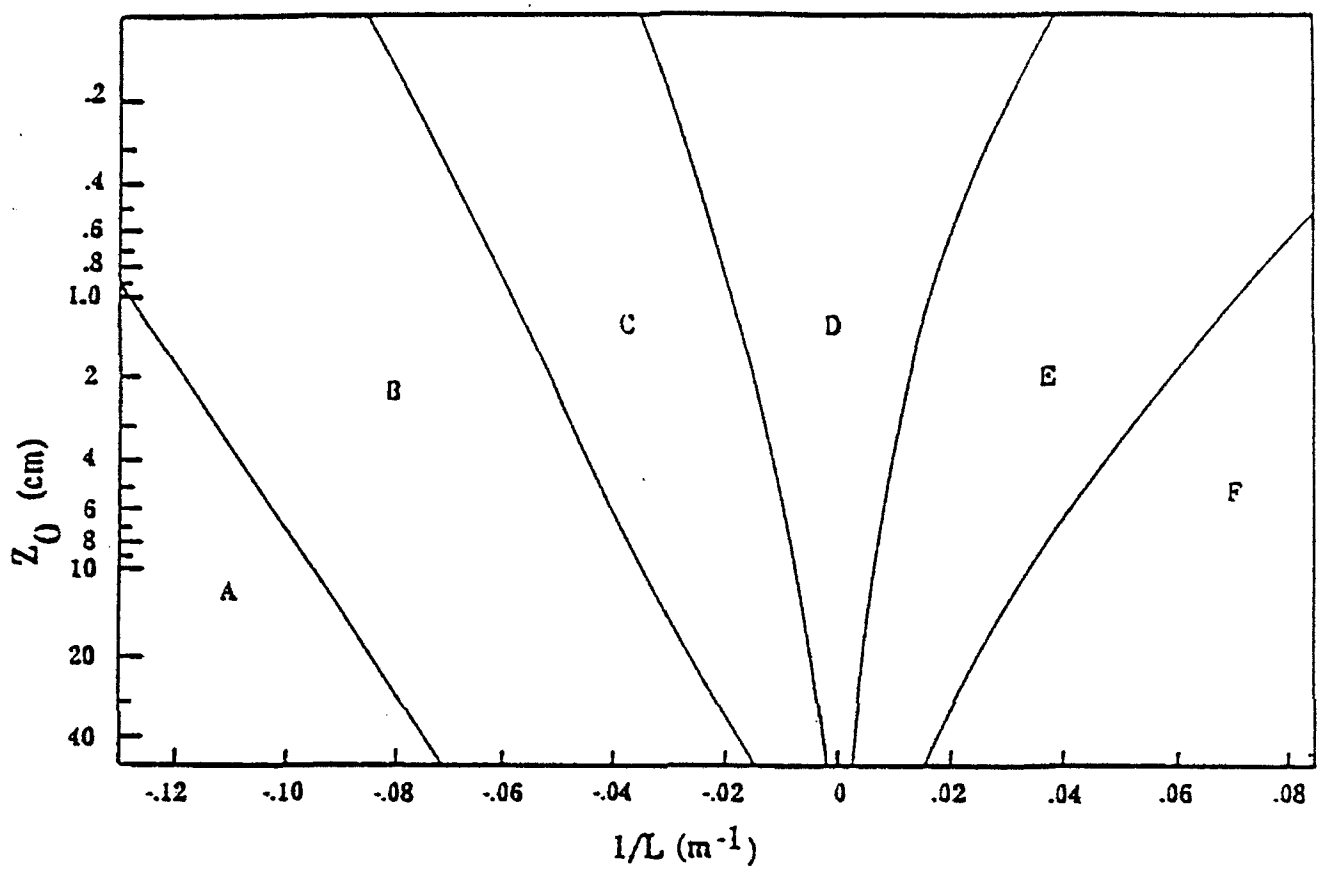

Figure 18. Pasquill stability classes as a function of inverse Monin-Obukhov length (1/L) and surface roughness length (z_o). (Golder, 1972).

Table 6

Power Law coefficients Relating L to z_o in the Equation ($L^{-1} = a\ (z_o)^b$)
(From Irwin, 1979)

Pasquill Class	a	b
A	-0.11360	-0.1029
B	-0.03849	-0.1714
C	-0.00807	-0.3049
D	0.0	0.0
E	0.00807	-0.3049
F	0.03849	-0.1714

$$L = \left\{ (a_1 P + a_2 P^3)\, z_o^{-(b_1 - b_2|P| + b_3 P^2)} \right\}^{-1} \qquad (52)$$

where the empirical constants are $a_1 = 0.004349$, $a_2 = 0.003724$, $b_1 = 0.5034$, $b_2 = 0.2310$, and $b_3 = 0.0325$.

Bowling (1985) pointed out the importance of snow cover in determining atmospheric stability at high latitudes. Also, the effect of latitude on solar elevation angle on Pasquill stability was determined by Andrews and Hansen (1988). Hansen (1990) developed a fractional stability scheme combining which provides greater resolution to the subjective Pasquill classes as well as a method to estimate the Monin-Obukhov length. This scheme has been incorporated into the FSCAT computer model (Pena and Sutter, 1990).

Another measure of stability is the Kazanski-Monin parameter, μ, defined as (Kazanski and Monin, 1960):

$$\mu = \frac{g\, k^2\, Q_h}{f\, \rho\, c_p\, T\, u_*^2} \qquad (53)$$

where g is the acceleration due to gravity,
k is the von Karman constant,
Q_h is the surface sensible heat flux,
f is the Coriolis parameter,
ρ is the air density,
c_p is the specific heat of air at constant pressure,
T is the ambient temperature, and,
u_* is the surface friction velocity.

Smith (1979) developed an empirical relationship relating μ to Pasquill class, P for unstable and neutral cases and for a surface roughness length of 10 cm:

$$P = \frac{3.6}{1 - 0.53(\mu/100) + 4.9(\mu/100)^2 + 2.0(\mu/100)^3} \qquad (54)$$

Sutherland et al. (1986) defined a modified version of the Kazanski-Monin parameter, μ', which included an explicit surface roughness factor:

$$\mu' = -\alpha(z_o) \frac{g\, k^2\, Q_h}{2\Omega\, \rho\, c_p\, T\, u_*^2} \qquad (55)$$

where $\alpha(z_o) = [a \ln(b/z_o)]^{-1}$ and a, b are empirical constants.

Sutherland et al. (1986) developed a simple exponential relationship relating μ' to the Pasquill class P:

$$P = A\, e^{\mu'} \qquad (56)$$

The modified Kazanski-Monin parameter eliminates problems with μ at low latitudes associated with the Coriolis parameter in the denominator of Eqn. (53), and is more general than Eqn. (54) in that it applies to any stability class and roughness length.

Sedefian and Bennett (1980) compared the results of several schemes for estimating atmospheric stability, including methods based on the standard deviation of horizontal wind fluctuations (σ_θ method), temperature difference at two heights (ΔT method), Richardson number and bulk Richardson number methods, and Turner (1964) method. Their results indicated a poor correlation between the various methods on an hourly basis, and they suggested the need to relate plume dispersion coefficients directly to the parameters used to turbulence parameters.

Weil and Brower (1984) use the ratio of the mean wind speed to the convective velocity scale (i.e., u/w_*) as a stability parameter rather than the Turner class during convective conditions. Their model, the Maryland Power Plant Siting Program (PPSP) model applies to tall stacks over flat terrain. They use rural Briggs dispersion coefficients for elevated sources in rural areas with the ratio u/w_* determining the effective stability class. During nighttime hours, the Turner stability class scheme is used. Their stability criteria are shown in Table 7. In urban areas, the same daytime

Table 7

Stability Scheme for Selecting Dispersion Parameters in the PPSP Model for Rural Areas

(From Weil and Brower, 1984)

Day	u/w_* criteria	Briggs curve
	$u/w_* < 3.5$	A
	$3.5 \leq u/w_* < 6.0$	B
	$6.0 \leq u/w_* < 13.9$	C
	$13.9 \leq u/w_*$	D
Night	**Turner stability class**	**Briggs curve**
	D	D
	E	E
	F	F
	G	F

stability scheme is used with the urban Briggs curves, but at night, urban Briggs D curves are applied for all nighttime Turner stability classes. Some of the concepts used by Weil and Brower are discussed in more detail in Section 3.2.

Briggs (1988) also concluded that the ratio u/w_* is a useful measure of dispersion rates in moderately to very unstable conditions. He suggested that convective scaling provides the best framework for evaluating the effects of urban scale surface inhomogeneities on dispersion rates in convective conditions.

Segal et al. (1990) examined the effects of surface evaporation rates on Pasquill classes and the scaling parameter u/w_*. Their results suggested that increased surface moisture has a significant impact on shifting stability toward more neutral conditions as measured by either stability index. High surface moisture also resulted in significantly lower daytime mixing heights (by a factor of 1.5 to 2.0) than low surface moisture conditions. These results are attributed to a shifting of available energy away from sensible heat into latent heat with higher values of surface moisture.

The EPA Industrial Source Complex (ISC) model accounts for differences in surface characteristics on dispersion rates by employing two sets of dispersion curves: the Pasquill-Gifford (PG) curves for rural areas and the McElroy-Pooler (MP) curves for urban areas. The MP curves are based on field experiments conducted in the St. Louis urban area. The Briggs curve (Gifford, 1976) fit to the St. Louis tracer data are used to define the urban dispersion coefficients in the model. The Turner (1964) stability classification scheme is used in ISC with either PG or MP dispersion coefficients. In urban mode with the MP coefficients, ISC combines stability classes A-B and E-F, resulting in four separate dispersion classes. In rural mode, six stability classes (A-F) are used. The EPA procedure is to combine Turner classes 6 and 7 into class F.

One of the difficulties with the use of a discrete stability class scheme and dispersion curves to characterize dispersion is the discontinuous

nature of the predicted concentrations as a function of stability class and surface type. In addition, because the PG curves were derived from near-ground level releases over relatively flat terrain (z_o ~ 3 cm) and measured only over short downwind distances (i.e., < 1 km), their application to conditions outside this range of conditions, especially to plumes emitted from tall stacks, is questionable (Hanna et al., 1977).

In recent years, the trend in dispersion modeling has been to parameterize turbulence (and dispersion) directly in terms of measured or derived meteorological variables using boundary layer theory. For example, the AMS workshop of stability classification schemes (Hanna et al., 1977) suggested the use of the standard deviations of the crosswind component (σ_v) and vertical component (σ_w) of the wind to estimate the plume dispersion parameters σ_y and σ_z:

$$\sigma_y = \sigma_v \, t \, f_y \tag{57}$$

$$\sigma_z = \sigma_w \, t \, f_z \tag{58}$$

where t is time for the pollutant to travel to the receptor,

σ_y, σ_z are the standard deviations of the horizontal and vertical components of the pollutant concentration distribution, respectively,

f_y, f_z are nondimensional functions.

In the next section, methods to estimate σ_v, σ_w, f_y, and f_z based on boundary layer theory are described.

3.2 Similarity Relations for Atmospheric Turbulence and Dispersion Parameters

A number of different scaling laws have been developed to apply over various regions of the atmospheric boundary layer or during particular stability conditions. The basic approach is to represent boundary layer properties in terms of a limited number of characteristics scaling parameters. Holtslag and Nieuwstadt (1986) have summarized the various regimes and the scaling parameters which apply in terms of two diagrams (see Figure 19 for unstable conditions and Figure 20 for the stable boundary layer). The scaling parameters used in the figures are:

L - Monin-obukhov length,

h - mixing height,

z - height above the ground,

$\overline{w\theta}_o$ - surface height flux,

τ_o - surface stress ($= \rho u_*^2$), and,

Λ - local length scale in the stable boundary layer

Weil (1985) and Briggs (1985) provide reviews on the use of similarity theory in diffusion models. In the convective boundary layer, Weil describes the turbulence characteristics in three layers:

(1) Surface layer: $z \leq 0.1\ h$ — σ_v ~ constant with height; σ_w increases with height

(2) Mixed layer: $0.1\ h < z < 0.8\ h$ — σ_v ~ constant with height; σ_w ~ constant with height

(3) Entrainment layer: $z > 0.8h$ — σ_v decreases with height; σ_w decreases with height.

In the surface layer, Panofsky et al. (1977) propose the following relations.

$$\sigma_v = u_* \left[4 + 0.6\ (-h/L)^{2/3} \right]^{1/2} \tag{59}$$

$$\sigma_w = u_* \left[1.6 + 2.9\ (-z/L)^{2/3} \right]^{1/2} \tag{60}$$

Hicks (1985) suggests the following for the convective mixed layer (0.1 to 0.8 h).

$$\sigma_v = \left(3.6\ u_*^2 + 0.35\ w_*^2 \right)^{1/2} \tag{61}$$

$$\sigma_w = \left(1.2\ u_*^2 + 0.35\ w_*^2 \right)^{1/2} \tag{62}$$

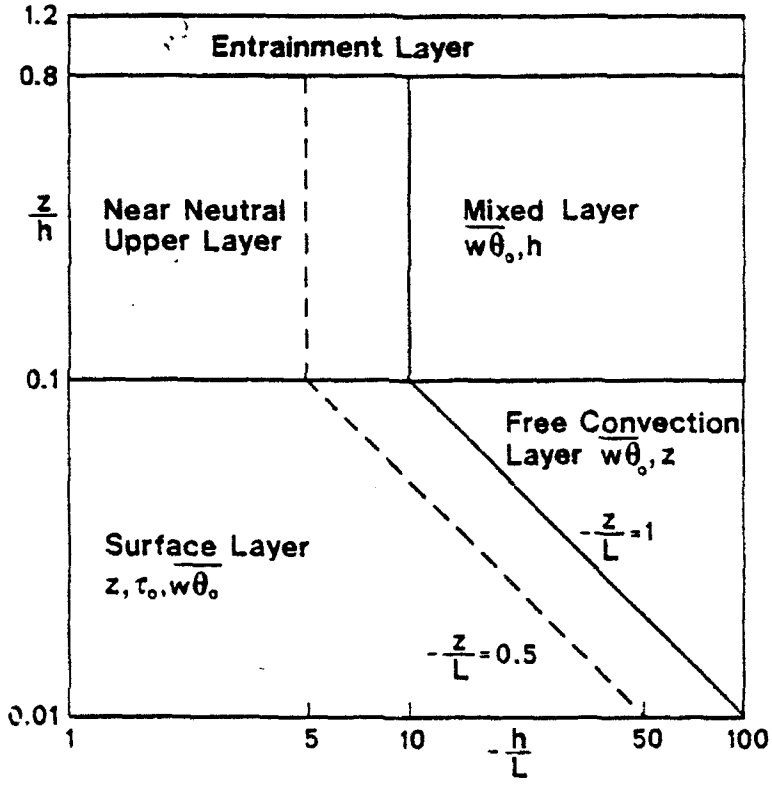

Figure 19.. Definitions of scaling regimes in the unstable atmospheric boundary layer (L < 0). (From Holtslag and Nieuwstadt, 1986).

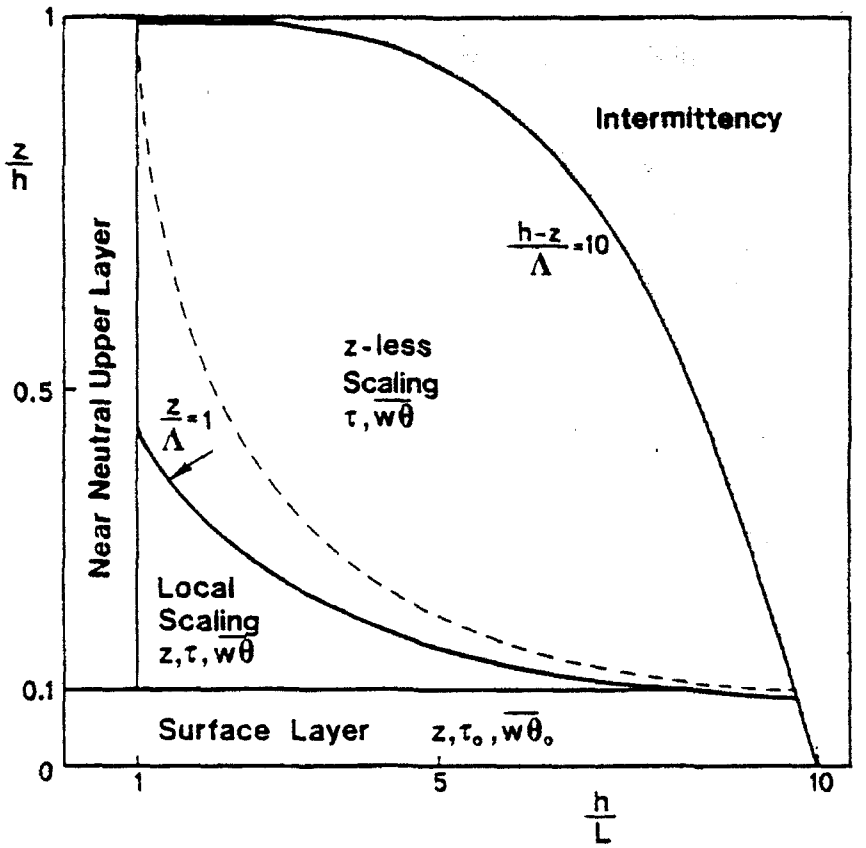

Figure 20. Definitions of scaling regimes in the stable atmospheric boundary layer (L > 0). The dashed line is z/L = 1. (From Holtslag and Nieuwstadt, 1986).

In the neutral boundary layer, Arya (1984) reports monotonically decreasing values of σ_v and σ_w throughout the mixed layer. Using Blackadar and Tennekes (1968) relationship for the neutral boundary layer height, Arya's results can be expressed as:

$$\sigma_v = 1.8\, e^{-0.9(z/h)} \tag{63}$$

$$\sigma_w = 1.3\, e^{-0.9(z/h)} \tag{64}$$

In the stable boundary layer, Nieuwstadt (1984) finds that σ_v and σ_w bear constant ratios with the local friction velocity.

$$\sigma_v/u_{*l} = C_v \tag{65}$$

$$\sigma_w/u_{*l} = C_w \tag{66}$$

where u_{*l} is the local friction velocity, and,
C_v and C_w are constants.

Hanna et al. (1986) suggest that $C_v \approx 1.6$. C_w has a value ≈ 1.3 (Nieuwstadt, 1984). The local friction velocity, u_{*l}, can be expressed (Nieuwstadt, 1984) as:

$$u_{*l} = u_* (1 - z/h)^{3/4} \tag{67}$$

The above equations represent the scaling relations appropriate for each layer for convective, neutral, and stable conditions. However, in order to provide a smooth transition from one vertical layer or stability regime to another, a set of combined, interpolation formulas have been developed (Scire et al., 1990b). These equations yield the proper values and vertical variations in the convective, neutral, and stable limits while providing a mechanism for interpolating the results for intermediate conditions without physically unrealistic discontinuities. The following equations, based on the relations presented above, apply for the neutral-convective boundary layer. The formulation for the entrainment layer is based on data reported by Caughey (1981).

Surface Layer: $z \leq 0.1\ h$ $(L \leq 0)$

$$\sigma_v = \left[4\ u_*^2\ a_n^2 + 0.35\ w_*^2 \right]^{1/2} \tag{68}$$

$$\sigma_w = \left[1.6\ u_*^2\ a_n^2 + 2.9\ u_*^2\ (-z/L)^{2/3} \right]^{1/2} \tag{69}$$

$$a_n = e^{-0.9(z/h)} \tag{70}$$

Mixed Layer: $z = 0.1\ h$ to $0.8\ h$ $(L \leq 0)$

$$\sigma_v = \left[4\ u_*^2\ a_n^2 + 0.35\ w_*^2 \right]^{1/2} \tag{71}$$

$$\sigma_w = \left[1.15\ u_*^2\ a_n^2 + 0.35\ w_*^2 \right]^{1/2} \tag{72}$$

Entrainment Layer: $z > 0.8\ h$ $(L \leq 0)$

$$\sigma_v = \left[4\ u_*^2\ a_n^2 + 0.35\ w_*^2 \right]^{1/2} \tag{73}$$

For $z = 0.8\ h$ to $1.2\ h$:

$$\sigma_w = \left[1.15\ u_*^2\ a_n^2 + a_{c1}\ 0.35\ w_*^2 \right]^{1/2} \tag{74}$$

$$a_{c1} = \left[0.5 + (h-z)/(0.4h) \right] \tag{75}$$

For $z = 1.0\ h$ to $1.2\ h$:

$$\sigma_w = \left[1.15\ u_*^2\ a_n^2 + a_{c2}\ 0.35\ w_*^2 \right]^{1/2} \tag{76}$$

$$a_{c2} = \left[1/3 + (1.2h - z)/(1.2\ h) \right] \tag{77}$$

In the neutral-stable boundary layer, the following equations are used to interpolate vertical profiles of σ_v and σ_w as a function of stability. They provide the proper values in both the neutral and stable limits.

$$\sigma_v = u_* \left[(1.6\ C_s\ (z/L) + 1.8\ a_n)/(1 + z/L) \right] \qquad (L > 0) \qquad (78)$$

$$\sigma_w = 1.3\ u_* \left[(C_s\ (z/L) + a_n)/(1 + z/L) \right] \qquad (L > 0) \qquad (79)$$

$$C_s = (1 - z/h)^{3/4} \qquad (L > 0) \qquad (80)$$

In order to provide for non-zero plume growth rates above the mixing height and to prevent numerical problems within the dispersion calculations associated with near-zero plume dimensions, minimum σ_v and σ_w values can be assigned. Hanna et al., (1986) suggest that an appropriate minimum one-hour average σ_v value is $\simeq$ 0.5 m/s.

Equations (68) to (77) have been tested with the original data providing the basis for the Panofsky et al. (1977) and Hicks (1985) formulations. The results, summarized in Table 8, indicate that the modified equations compare well with the original equations and the observational data. The modified equations have the advantage of a smooth and continuous transition to the neutral results of Arya (1984).

Irwin (1983) has evaluated several schemes for determining the f_y and f_z functions, including equations suggested by Draxler (1976), Pasquill (1976), and Cramer (1976). His conclusion was that the parameterization suggested by Draxler (1976) performed best overall.

$$f_y = \left[1 + 0.9\ (t/1000)^{1/2} \right]^{-1} \qquad (81)$$

$$f_z = \begin{cases} \left[1 + 0.9\ (t/500)^{1/2} \right]^{-1} & (L < 0) \qquad (82) \\ \left[1 + 0.945\ (t/100)^{0.806} \right]^{-1} & (L > 0) \qquad (83) \end{cases}$$

These relations provide a mechanism for determining atmospheric turbulence and dispersion rates in a continuous manner as a function of stability and plume height.

Table 8

Comparison of Panofsky et al. (1977) and Hicks (1985)
Formulations of σ_v and σ_w with Equations (68)-(77)
(From Scire et al., 1990)

Panofsky et al. data	Observed σ_v vs. Panofsky	Observed σ_v vs. Eqns. (68)-(77)	Panofsky σ_v vs. Eqns. (68)-(77)
Averages	(1.14, 1.20)	(1.14, 1.21)	(1.20, 1.21)
Corr. Coef.	.81	.84	.992
Average Bias	.07	.07	.00
Average Abs. Error	.10	.09	.02
RMSE	.13	.12	.02

Hicks 1985 data	Observed σ_v vs. Hicks	Observed σ_v vs. Eqns. (68)-(77)	Hicks σ_v vs. Eqns. (68)-(77)
Averages	(1.17, 1.12)	(1.17, 1.06)	(1.12, 1.06)
Corr. Coef.	.79	.77	.998
Average Bias	-.05	-.11	.06
Average Abs. Error	.20	.23	.06
RMSE	.27	.30	.08

Hicks 1985 data	Observed σ_w vs. Hicks	Observed σ_w vs. Eqns. (68)-(77)	Hicks σ_w vs. Eqns. (68)-(77)
Averages	(0.98, 1.01)	(0.98, 0.98)	(1.01, 0.98)
Corr. Coef.	.91	.91	.998
Average Bias	.03	.00	-.03
Average Abs. Error	.12	.11	.03
RMSE	.15	.14	.04

4. CONCLUSIONS AND RECOMMENDATIONS

In this Phase I effort, a detailed methodology appropriate for estimating stability and dispersion parameters in an urban environment has been described. The main advantages of the approach include the ability to provide continuous estimates of stability and dispersion as a function of stability, plume height, and surface characteristics, the requirement for only routinely-available meteorological inputs and land use data, and computational efficiency (i.e., it is designed to run on a PC).

The major components of the model are a new soil moisture model capable of predicting surface wetness factors over both rural and urban land use types, a meteorological preprocessor which computes heat fluxes and boundary layer scaling parameters, and a set of similarity relationships to estimate atmospheric stability and plume dispersion rates. The various components of the model have been coded and subjected to module testing. Among the conclusions and recommendations of the Phase I literature review and development effort are:

(1) The surface moisture parameter is a critical input to the energy balance scheme of Holtslag and van Ulden (1983). It is also one of the most difficult to specify because it exhibits considerable spatial and time variability, reflecting differences in land use and the variability of precipitation.

(2) A simple two-capacitor soil moisture model has shown the ability to reproduce the behavior of more complex numerical models during simulated drying out periods. Sample simulations of a three month period for both rural and urban areas produce qualitatively reasonable results. Further testing and enhancement of the capacitance model with the Indianapolis urban data base is recommended. The testing should focus on two issue: 1) Do observed heat fluxes show the expected behavior during periods with no precipitation? (i.e., a shift from latent to sensible heat flux with time); 2) Is the capacitance model able to more accurately predict energy fluxes than the use of constant, time-averaged values of the soil moisture parameter?

(3) The soil moisture model contains several parameters which need to be determined empirically. These include the capacitor time constants (τ) and minimum/maximum capacitor change (q). Additional work needs to be done to (1) evaluate if the number of parameters can be reduced and (2) determine recommended values for the parameters based on routinely available information (e.g., land use types).

(4) A method for including the buoyancy effects of water vapor on boundary layer parameters has been described. Further testing is recommended to quantify the magnitude of these effects and the conditions under which they are likely to be important.

(5) A well-known surface energy balance method, adapted for urban conditions, but also applicable to suburban and rural land surfaces as well, has been demonstrated. The method is well suited for further study and development. It requires only routinely available data inputs and produces the boundary layer parameters required by state-of-the-science scaling techniques to estimate stability and plume dispersion rates. It is recommended that the performance of the coupled capacitance-meteorological model be assessed in future Phase II work. The Indianapolis and St. Louis data sets are suitable candidates for this evaluation effort.

(6) A number of schemes to estimate Pasquill stability classes have been reviewed. The use of scaling techniques is recommended to provide a continuous estimate of dispersion and stability parameters consistent with current boundary layer similarity theory.

(7) A series of scaling equations describing the turbulence parameters, σ_v and σ_w, in various scaling regimes (height and stability regimes) have been presented. Two sets of interpolation formulas which provide for a smooth and continuous variation of the turbulence parameters from one regime to another have been described. The first set deals with the unstable to neutral regime, and the second handles the stable to neutral transition.

Further refinement and testing of these formulas is recommended in a Phase II effort.

(8) Once the three major modules of the model have been tested further, it is recommended that the components be integrated into a single system and tested as a unit in Phase II work. An user-friendly front-end input module should be included to facilitate its use. The predicted dispersion parameters are suitable for coupling directly to a dispersion model.

This Phase I study has demonstrated the feasibility of a pc-based modeling system for predicting urban (and rural) stability and atmospheric turbulence parameters in a continuous manner based on the use of only routinely-available input data. The actual development of an integrated system and further testing of the system components and the completed unit are recommended as a potential Phase II development project.

REFERENCES

Acs, F., D.T. Mihailovic and B. Rajkovic, 1991: A coupled soil moisture and surface temperature prediction model. *J. Appl. Meteor.*, 30, 812-822.

Andrews, J.A., and F.V. Hansen, 1989: The Pasquill stability categories: A decision tree solution. U.S. Army Atmospheric Sciences Laboratory, White Sands Missile Range, NM.

Arya, S.P.S., 1984: Parametric relations for the atmospheric boundary layer. *Boundary Layer Meteor.*, 30, 57-73.

Arya, S.P.S., 1988: *Introduction to Micrometeorology*. Academic Press, New York, NY.

Auer, A.H. Jr., 1978: Correlation of land use and cover with meteorological anomalies. *J. Appl. Meteor.*, 17, 636-643.

Berkowitz, R., and L.P. Prahm, 1982: Sensible heat flux estimated from routine meteorological data by the resistance method. *J. Appl. Meteor.*, 21, 1845-1864.

Blackadar, A.K., and H. Tennekes, 1968: Asymptotic similarity in neutral barotropic planetary boundary layers. *J. Atmos. Sci.*, 25, 1025-1020.

Bowling, S.A., 1985: Modifications necessary to use standard dispersion models at high latitudes. *Atmos. Environ.*, 19, 93-97.

Briggs, G.A., 1973: *Diffusion Estimates for Small Emissions* (Draft). Air Resources Atmospheric Turbulence and Diffusion Laboratory. ATOL No. 79.

Briggs, G.A., 1982: Simple substitutes for the Obukhov length. Proceedings, 3rd Joint Conference on Appl. of Air Poll. Meteor., American Meteorological Society, Boston, MA, 68-71.

Briggs, G.A., 1983: Diffusion modeling with convective scaling. Urban scale variations of turbulence parameters and fluxes. American Meteorological Society Specialty Conference on Air Quality Modeling of the Urban Boundary Layer, Baltimore, MD.

Briggs, G.A., 1985: Analytical parameterizations of diffusion: The Convective Boundary Layer. *J. Clim. and Appl. Meteor.*, 24, 1167-1186.

Briggs, G.A., 1988: Surface inhomogeneity effects on convective diffusion. *Boundary Layer Meteor.*, 45, 117-135.

Carson, D.J., 1973: The development of a dry inversion-capped convectively unstable boundary layer. *Quart. J. Roy. Meteor. Soc.*, 99, 450-467.

Caughey, S.J., 1981: Observed Characteristics of the Atmospheric Boundary Layer. In *Atmospheric Turbulence and Air Pollution Modeling*, F.T.M. Nieuwstadt and H. Van Dop, Eds. D. Reidel Publishing Company, Boston, MA.

Ching, J.K.S., J.F. Clarke, and J.M. Godowitch, 1978: "The variability of the heat flux and mixed layer depth over St. Louis, MO," *WMO Symp, Boundary Layer Physics Applied to Special Problems of Air Pollution*. WMO No. 510, Geneva, 71-78.

Ching, J.K.S. J.M. Godowitch, J.F. Clarke and A.H. Auer, 1983: Urban scale variations of turbulence parameters and fluxes. *AMS Specialty Conference on Air Quality Modeling of the Urban Boundary Layer*, Baltimore, MD.

Cleugh, H.A., and T.R. Oke, 1986: Suburban-rural energy balance comparisons in summer for Vancouver, C.C. *Boundary Layer Meteor.*, **36**, 351-369.

Coulson, K.L., and D.W. Reynolds, 1971: The spectral reflectance of natural surfaces. *J. Appl. Meteor.*, **10**, 1285-1295.

Cramer, H.E., 1976: Improved techniques for modeling the dispersion of tall stack plumes. *Proc. 7th Int. Technical Meeting on Air Pollution Modeling and its Application*, N. 51, NATO/CCMS, 731-780.

Deardorff, J.W., 1977: A parameterization of ground-surface moisture content for use in atmospheric prediction models. *J. Appl. Meteor.*, **16**, 1182-1185.

Deardorff, J.W., 1978: Efficient prediction of ground surface temperature and moisture with inclusions of a layer of vegetation. *J. Geophys. Res.*, **83**, 1889-1903.

Deardorff, J.W., 1980: Progress in understanding entrainment at the top of a mixed layer. *Proceedings Workshop on the Planetary Boundary Layer*, J.C. Wyngaard, Ed., American Meteorological Society, 36-66.

Deardorff, J.W., and G.E. Willis, 1975: A parameterization of diffusion into the mixed layer. *J. Appl. Meteor.*, **14**, 1451-1458.

DeBruin, H.A.R., and A.A.M. Holtslag, 1982: A simple parameterization of the surface fluxes of sensible and latent heat during daytime compared with the Penman-Monteith concept. *J. Clim. Appl. Meteor.*, **21**, 1610-1621.

Draxler, R.R., 1976: Determination of atmospheric diffusion parameters. *Atmos. Environ.*, **10**, 99-105.

Dyer, A.J., and B.B. Hicks, 1970: Flux-gradient relationships in the constant flux layer. *Quart. J. Roy. Meteor. Soc.*, **96**, 715-721.

Gifford, F.A., Jr., 1976: Turbulent Diffusion--Typing schemes: A Review. *Nucl. Saf.*, **17**, 68-86.

Godowitch, J.M., J.K.S. Ching, and J.F. Clarke, 1981: Urban/rural and temporal variations in PBL turbulence parameters and length scales over St. Louis, MO. American Meteorological Society Fifth Symposium on Turbulence, Diffusion, and Air Pollution, March 9-13, Atlanta, GA.

Golder, D.G., 1972: Relations among stability parameters in the surface layer. *Boundary Layer Meteor.*, 3, 47-58.

Hanna, S.R., G.A. Briggs, J. Deardorff, B.A. Egan, F.A. Gifford and F. Pasquill, 1977: American Meteorological Society Workshop on Stability Classification Schemes and Sigma Curves - Summary of Recommendations. *Bull. Am. Meteor. Soc.*, 58, 1305-1309.

Hanna, S.R., G.A. Briggs and R.P. Hosker, 1982: *Handbook on Atmospheric Diffusion.* NTIS DE82-002045, Technical Information Center, U.S. Department of Energy,. Washington, DC.

Hanna, S.R., and J.C. Chang, 1990: Modification of the Hybrid Plume Dispersion Model (HPDM) for urban conditions and its evaluation using the Indianapolis data set. Vol. III. Analysis of urban boundary layer data. Sigma Research Corporation, Westford, MA.

Hanna, S.R., and J.C. Chang, 1991: Modification of the Hybrid Plume Dispersion Model (HPDM) for urban conditions and its evaluation using the Indianapolis data set. Vol. I. User's guide for HPDM-Urban. Sigma Research Corporation, Westford, MA.

Hanna, S.R., and J.C. Chang, 1992: Boundary-layer parameterizations for applied dispersion modeling over urban areas. *Bound. Lay. Meteorol.*, 58, 229-259.

Hanna, S.R., J.C. Weil and R.J. Paine, 1986: *Plume Model Development and Evaluation.* Report Number D034-500. Electric Power Research Institute, Palo Alto, CA.

Hansen, F.V., 1990: A fractional stability category scheme. U.S. Army Atmospheric Sciences Laboratory, White Sands Missile Range, NM.

Hicks, B.B., 1985: Behavior of Turbulence Statistics in the Convective Boundary Layer. *J. Clim. and Appl. Meteor.*, 24, 607-614.

Hildebrand, P.H.,and B. Ackerman, 1984: Urban effects on the convective boundary layer. *J. Atmos. Sci.*, 41, 76-91.

Holtslag, A.A.M., and F.T.M. Nieuwstadt, 1986: Scaling the atmospheric boundary layer. *Boundary Layer Meteor.*, 36, 201-209.

Holtslag, A.A.M., and A.P. van Ulden, 1983: A simple scheme for daytime estimates of the surface fluxes from routine weather data. *J. Climate & Appl. Meteor.*, 22, 517-529.

Iqbal, Muhammad, 1983: *An Introduction to Solar Radiation.* Academic Press, 286.

Irwin, J.S., 1979a: Estimating plume dispersion--A recommended generalized scheme. *Fourth Symposium on Turbulence, Diffusion and Air Pollution,* American Meteorological Society, Boston, MA, Boston, MA.

Irwin, J.S., 1979b: *Scheme for Estimating Dispersion Parameters as a Function of Release Height.* EPA-600/4-79-062, U.S. Environmental Protection Agency, Research Triangle Park, NC.

Irwin, J.S., 1983: Estimating Plume Dispersion--A Comparison of Several Sigma Schemes. *J. Clim. and Appl. Meteor.*, 22, 92-114.

Jackson, R.D., 1973: Diurnal changes in soil water content during drying. Field Soil Water Regime. *Soil Sci. Soc. Amer.*, 37-55.

Kato, H., and O.M. Phillips, 1969: On the penetration of a turbulence layer into a stratified fluid. *J. Fluid Mech.*, **37**, 643-655.

Kazanski, A.B., and A.S. Monin, 1960: A turbulent regime above the surface atmospheric layer. *Izv. Acad. Sci., USSR, Geof. Ser.*, 1, 110.

Kimura, F., and S. Takahashi, 1991: The effects of land-use and anthropogenic heating on the surface temperature in the Tokyo metropolitan area: A numerical experiment. *Atmos. Environ.*, **25B**, 155-164.

Lamb, R.G., 1981: Diffusion in the Convective Boundary Layer. In *Atmospheric Turbulence and Air Pollution Modeling*, T.F.M. Nieuwstadt and K. van Dop, eds. D. Reidel Publishing Company, Boston, MA.

Landsberg, H.E., 1981: The Urban Heat Island. Academic Press. New York, NY.

Liu, M.K., D.R. Durran, P. Mundkur, M. Yocke and J. Ames, 1976: The chemistry, dispersion, and transport of air pollutants emitted form fossil fuel power plants in California, Data analysis and emission impact model. ARB-R-4-258-276-54, Systems Applications, Inc., San Rafael, CA.

McElroy, J.L., and F. Pooler, 1968: The St. Louis dispersion study. U.S. Public Health Service, National Air Pollution Control Administration, Report AP-53.

McGoldrick, B. 1980: Artificial heat release from Greater London, 1971. Physics Div. Energy Workshop Report No. 20, 32 pp., Dept. of Physical Sciences, Sunderland Polytechnic, Sunderland.

Nieuwstadt, F.T.M., 1981: The steady-state height and resistance laws of the nocturnal boundary layer: Theory compared with Cabauw observations. *Boundary Layer Meteor.*, **20**, 3-17.

Nieuwstadt, F.T.M., 1984: Some aspects of the turbulent stable boundary layer. *Boundary Layer Meteor.*, **30**, 31-55.

Noilhan, J., and S. Planton, 1989: A simple parameterization of land surface processes for meteorological models. *Mon. Wea. Rev.*, 17, 536-549.

Oke, T.R., 1978: *Boundary Layer Climates*. John Wiley & Sons, New York, NY.

Oke, T.R., 1982: The energetic basis of the urban heat island. *Quart. J.R. Meteor. Soc.*, **108**, 1-24.

Pan, H.-L., and L. Mahrt, 1987: Interaction between soil hydrology and boundary-layer development. *Boundary Layer Meteor.*, **38**, 185-202.

Panofsky, H.A., H. Tennekes, D.H. Lenschow and J.C. Wynngaard, 1977: The characteristics of turbulent velocity components in the surface layer under convective conditions. *Boundary Layer Meteor.*, **11**, 355-361.

Pasquill, F., 1961: The estimation of the dispersion of windborne material. *Meteor. Mag.*, **90**, 33-49.

Pasquill, F., 1976: *Atmospheric Dispersion Parameters in Gaussian Plume Modeling: Part II. Possible Requirements for Change in the Turner Workbook Values.* EPA-600/4-76-030b, U.S. Environmental Protection Agency, Research Triangle Park, No. Carolina. 53 pp.

Pena, R., and D. DeSutter, 1990: FSCAT: A fractional stability category computer code. U.S. Army Atmospheric Sciences Laboratory, White Sands Missile Range, NM.

Scire, J.S., D.C. DiCristofaro, and D.G. Strimaitis, 1986: Development and application of a deposition modeling approach for PCDD and PCDF emissions from the proposed Brooklyn Navy Yard Resource Recovery Facility. Sigma Research Corporation, Westford, MA.

Scire, J.S., E.M. Insley and R.J. Yamartino, 1990a: Model formulation and user's guide for the CALMET meteorological model. Sigma Research Corporation, Westford, MA.

Scire, J.S., D.G. Strimaitis and R.J. Yamartino, 1990b: Model formulation and user's guide for the CALPUFF dispersion model. Sigma Research Corporation, Westford, MA.

Scire, J.S., and D.L. Wojichowski, 1987: Modeling deposition and dispersion in an urban environment. M.A.S.S.-APCA 33rd Anniv. Technical Conference, Nov. 3-6, Atlantic City, NJ.

Sedefian, L., and E. Bennett, 1980: A comparison of turbulence classification schemes. *Atmos. Environ.*, **14**, 741-750.

Segal, M., X. Jia and R.A. Pielke, 1990: On the effect of daytime surface evaporation and pollution dispersion. *Atmos. Environ.*, **24A**, 1801-1811.

Sellers, P.J., Y Mintz, Y.C. Sud and A. Dalcher, 1986: A simple biosphere model (SIB) for use with general circulation models. *J. Atmos. Sci.*, **43**, 505-531.

Shir, C.C., and L.J. Shieh, 1974: A generalized urban air pollution model and its application to the study of SO_2 distributions in the St. Louis metropolitan area. *J. Appl. Meteor.*, 13, 185-204.

Smith, F.B., 1979: The relation between Pasquill stability P and Kazanski-Monin stability μ (in neutral and unstable conditions). *Atmos. Environ.*, 13, 879-881.

Stull, R.B., 1983: Integral scales for the nocturnal boundary layer. Part 1: Empirical depth relationships. *J. Clim. and Appl. Meteor.*, 22, 673-686.

Stull, Roland B. 1988: *An Introduction to boundary layer meteorology.* Klauer Academic Publishers, Boston, MA, 666 pp.

Sutherland, R.A., F.V. Hansen and W.D. Bach, 1986: A quantitative method for estimating Pasquill stability class from windspeed and sensible heat flux density. *Boundary Layer Meteor.*, 37, 357-369.

Tennekes, H., 1973: A model for the dynamics of the inversion above a convective boundary layer. *J. Atmos. Sci.*, 30, 558-567.

Turner, D.B., 1964: A diffusion model for an urban area. *J. Appl. Meteor.*, 3, 83-91.

Uno, I., S. Wakamatsu, H. Ueda and A. Nakamura, 1988: An observational study of the structure of the nocturnal urban boundary layer. *Boundary Layer Meteor.*, 45, 59-82.

Unsworth, M.H., and J.L. Monteith, 1972: Aerosol and solar radiation in Britain. *Quart. J.R. Meteor. Soc.*, 98, 778-797.

U.S. EPA, 1987: Industrial Source Complex (ISC) dispersion model user's guide--Second edition (revised). Volume 1. EPA-450/4-88-002a. U.S. Environmental Protection Agency, Research Triangle Park, NC.

Van Ulden, A.P., and A.A.M. Holtslag, 1983: "The stability of the atmospheric surface layer during nighttime." Reprints, *Sixth Symp. on Turbulence and Diffusion*. American Meteorological Society, Boston, MA, 257-260.

van Ulden, A.P., and A.A.M. Holtslag, 1985. Estimation of atmospheric boundary layer parameters for diffusion applications. *J. Clim. and Appl. Meteor.*, 24, 1196-1207.

Wang, I.T.,and P.C. Chen, 1980: Estimations of heat and momentum fluxes near the ground. *Proc. 2nd Joint Conf. on Applications of Air Poll. Meteor.*, American Meteorological Society, Boston, MA, 764-769.

Weil, J.C., 1985: Updating applied diffusion models. *J. Clim. Appl. Meteor.*, 24, 1111-1130.

Weil, J.C., and R.P. Brower, 1983: *Estimating Convective Boundary Layer Parameters for Diffusion Application*, Draft Report Prepared by Environmental Center, Martin Marietta Corp., for Maryland Dept. of Natural Resources.

Weil, J.C., and R.P. Brower, 1984: An updated Gaussian plume model for tall stacks. *J. Air Poll. Control Assoc.*, 34, 818-827.

White, J.M., F.D. Eaton and A.H. Auer, 1978: The net radiation budget of the St. Louis Metropolitan area. *J. Appl. Meteor.*, 17, 593-599.

Zilitinkevich, S.S., 1972: On the determination of the height of the Ekman boundary layer. *Boundary Layer Meteor.*, 3, 141-145.